Lappeenranta-Lahti University of Technology LUT
School of Engineering System
Mechanical Engineering
Master's Programme in Mechatronic System Design

Elena Pupysheva

MONITORING SYSTEM FOR THE PARTICLE DISTRIBUTION OF FLOCULATED RED MUD PULP

Examiners: Professor Heikki Handroos
As. Prof. Elmira Fedorova

Supervisors: Professor Heikki Handroos
As. Prof. Elmira Fedorova

ABSTRACT

Lappeenranta-Lahti University of Technology LUT
School of Engineering System
Mechanical Engineering
Master's Programme in Mechatronic System Design

Elena Pupysheva

Monitoring system for the particle distribution of flocculated red mud pulp

Master’s Thesis

73 pages, 41 figures, 11 tables

Examiners: Professor Heikki Handroos
As. Prof. Elmira Fedorova

Keywords: master’s thesis, metallurgy, Matlab, flocculates, floccules, aggregation, Bayer method, thickener, PBE, red mud.

The aim of this master's thesis is to develop a programmed part of monitoring system for the particle size distribution of red mud slurry on the case of OJSC UAZ RUSAL's red mud.

In the course of the work, a literature review and the analysis of existing research on the topic were conducted to confirm the relevance of the master’s thesis. In particular, the following aspects of the special and practical parts were touched upon: the study of the red mud thickening process, the study of the flocculation process and kinetics, the application of the population balance. A laboratory study of the flocculation of red mud slurry was carried out on a sample obtained from the production of OJSC UAZ RUSAL in 2020. The outcome of the practical part is the implementation of the software code of the monitoring system and its visual component. The economic part considers the feasibility of implementing a monitoring system at OJSC UAZ RUSAL.

ACKNOWLEDGEMENTS

I wish to acknowledge the St. Petersburg Mining University and the Lappeenranta University of Technology for providing me with the opportunity to study for a master double degree. In particular, I would like to thank the supervisors Professor Heikki Hadroos and Associate Professor Elmira Fedorova for help they provided during the theses research.

TABLE OF CONTENTS

LIST OF SYMBOLS AND ABBREVIATIONS

A'	Fragmentation parameter [$cm^{-1}sq^{-1}$]
α_{ij}	Koefficient of collision efficiency of floccules of diameters i and j
β_{ij}	Koefficient of frequency of floccules of diameters i and j
D	Particle diameter [m]
$d(c,i)$	The collisional diameter of agglomerate section i [μm]
D_f	Fractal dimension [μm]
d_p	Dimeter of spherical monodisperse particles [μm]
ϕ_t	Maximum volume concentration [% vol. frac]
g	Free fall acceleration [m/s^2]
G	Shear rate [1/s]
k_b	Koefficient to support dimensional matching [$cm^{-1}s^{-1}$]
μ_i	Liquid dynamic viscosity [Pa-s]
N_i	Concentration of floccules containing 2_{i-1} particles [g/l]
ρ_p	Particle density [kg/m^3]
ρ	Liquid density [kg/m^3]
S_i	Collapse intensity of floccules of diameter i
v_s	Resulting Stokes speed [m/s]
Γ_{ij}	Distribution function of collapse of floccules of diameter j to diameter i

ACS	Automatic Process Control System
CFD	Computational fluid dynamics
DE	Differential Equation
FCF	Free cash flow
IRR	Internal Rate of Return
LALLS	Low-angle laser light scattering
NPV	Net Present Value
ODE	Ordinary Differential Equation
PB	Population balance
PBE	Population balance equation
PI	Profitability Index
RM	Red mud
UAZ	Urals Aluminium Plant RUSAL, RUSAL-URAL

1. INTRODUCTION

A particular feature of alumina production in Russia is the use of both high quality and low-quality bauxite as raw materials, including production residues - mud. Among the problems of processing bauxite into alumina are the following factors:

- There is a shortage of high-quality bauxite in Russia;
- High cost of energy resources.

The current state of alumina production indicates the need to modify existing processing methods into more technologically advanced and highly efficient ones.

There are numerous studies on technologies for the integrated processing of bauxite raw materials, processing, and storage of red mud, which is still a technogenic waste. Research relating to the alkaline treatment of red mud to extract useful components from it is popular. This master's thesis is based on the process of alkaline treatment of red mud in thickeners to produce aluminum hydroxide.

Particle size has a strong influence on the thickening process. With increasing particle size, the settling speed of the slurry increases considerably. The leaching behaviour is directly influenced by the particle size of the slurry, which depends on the bauxite milling conditions. An important parameter that directly affects the quality of the resulting raw material for thickening processes is the grain size distribution of the flocculated or coagulated slurry. At the moment it is not possible to sample the aggregate slurry from the vats dynamically without particle breakdown, so it can be concluded that introducing virtual systems (virtual instrumentation) into the existing control systems and using a digital process twin to identify key parameters will simplify process control and reduce the economic cost of alumina production.

1.1 Relevance of the problem

A relevant topic for thickening processes is the monitoring of the particle size distribution of the flocculated or coagulated slurry. Flocculus size, weighted average and median diameters have a direct influence on the settling and thickening process, so installing particle size sensors in the vat or feeder cup will disrupt the process.

In the planned work it is supposed to use population balance model for creation of system of monitoring of particle size distribution of red mud slurry in the working tank of the thickener, for the subsequent correction of technological process.

Particulate processes are characterised by continuous and dispersed phases. The phases significantly affect the final product quality and process performance due to the distribution of properties caused by the fact that the phases are formed from particles with a distribution of properties.Particle forming processes are found in the following processes: crystallisation, agglomeration, grinding, dissolution, leaching, etc. The increased interest of metallurgical industries in obtaining valuable products from recycled raw materials confirms the need to focus on particle processes and how to improve their performance. Automated process control is known to improve process performance and reduce process and product instability.

1.2 Goals and delimitations

The purpose of this work is to implement a population balance equation to monitor the particle size distribution of red mud slurry.

- To study the technological process of red mud thickening;
- To Identify the input/output parameters of the thickening process;
- To study the design of the unit;
- To carry out patent search and literature review of existing methods of analysis of flocculation and aggregation process;
- To Conduct a laboratory study on a red slurry sample to obtain baseline data;
- Correlation of input/output parameters on the basis of data slice;
- To Implement the monitoring system programmatically in Matlab environment;
- To Implement a population balance equation to simulate the aggregation process;
- Carry out an analysis of the system's performance;
- Analyse the cost-effectiveness of the virtual appliance

1.3 Analysis of existing studies on the subject

1.3.1 Existing methods for particle sizing

Particle size analyzers are used for the determination and analysis of a wide spectrum of particle dimensions. The analyzers are used in both light and heavy industries: chemical, food, and cosmetic/pharmaceutical, metallurgical, etc.

Sieve analysis

The most fundamental of the existing analytical methods for determining particle size is sieve analysis. The main advantage of sieve analysis is the low cost of equipment. Sieve analysis is mainly used in the mining industry where there is no need for fine particles.

The main disadvantages of the method are.

- Emulsions and aerosols/sprays cannot be investigated by sieve analysis;
- Measurement of dry powders with particles smaller than 38 μm is rather problematic;
- Limitation on the materials to be measured. Clay, as a bound and agglomerated material, is difficult to measure;
- Low resolution, particles on the order of 0.3 μm cannot be detected;
- If the measuring time is increased, the results may be "underestimated", because particles with a slightly elongated or needle-shaped shape are oriented and pass through the sieve during the long sieving process. Therefore, the grinding time and the sieving method (shaking or vibration) must be strictly adhered to within the specified limits.
- Sieve analysis of elongated, needle-shaped or flat particles does not reproduce the true value of the weight distribution;
- Controlling the hole size of the sieves used for analysis is problematic.

Sediment analysis

Sedimentation analysis is the traditional method of particle size analysis. Depending on a number of factors this method is applicable in the range of 2-50 μm. The measurement principle in sedimentation analysis is based on Stoke's law and the recording of steady-state settling velocities.

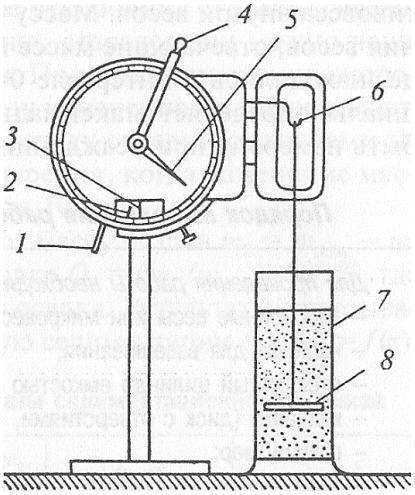

1 - scale arm; 2 - scale hand; 3 - risk; 4 - balancing lever; 5 - dial hand; 6 - cup hook; 7 - glass cylinder; 8 - scale cup

Figure 1. Schematic diagram of torsion scales

$$V_s = \frac{2}{9}\frac{r^2 g(\rho_p - \rho_f)}{\mu} \quad (1)$$

The equation 1 is the resulting Stokes speed, where ρ_p is particle density (kg/m^3),ρ is liquid density (kg/m3), D is particle diameter (m), g is free fall acceleration (m/s^2), μ is liquid dynamic viscosity (Pa-s).

To solve the equation above, the following factors must be taken into account: it is important to keep in mind the density of the dispersed phase. The particles have to settle, which is not suitable for emulsions where the sediment is stable. This approach is difficult for systems where the dispersed phase has a high density value (very high settling rate) or consists of materials with different densities.

The result is the Stokes diameter, which is the diameter of a sphere with the same settling velocity as the particle in question. The measurement requires accurate temperature control because the viscosity of the medium (in the denominator of the equation) is temperature dependent (about 2% deviation per 1ºC).

The main disadvantages of the method:

- Duration of the analysis. The analysis time may vary from 25 minutes to 1 hour which slows down the repeatability of the test and there is a high probability that material particles will tend to clump during the analysis;
- Maintaining a certain temperature. To control the temperature profile of the plant and viscosity changes, a high quality thermal stabilisation of the system is required;

- Materials with different densities can be analysed with low accuracy.
- Application of X-rays;
- Limited size range. Brownian motion begins to dominate in particles smaller than 2 μm, adding significant error to the analysis results. Whereas particles larger than 50 μm exhibit turbulence on settling, which prevents the use of Stokes' Law.

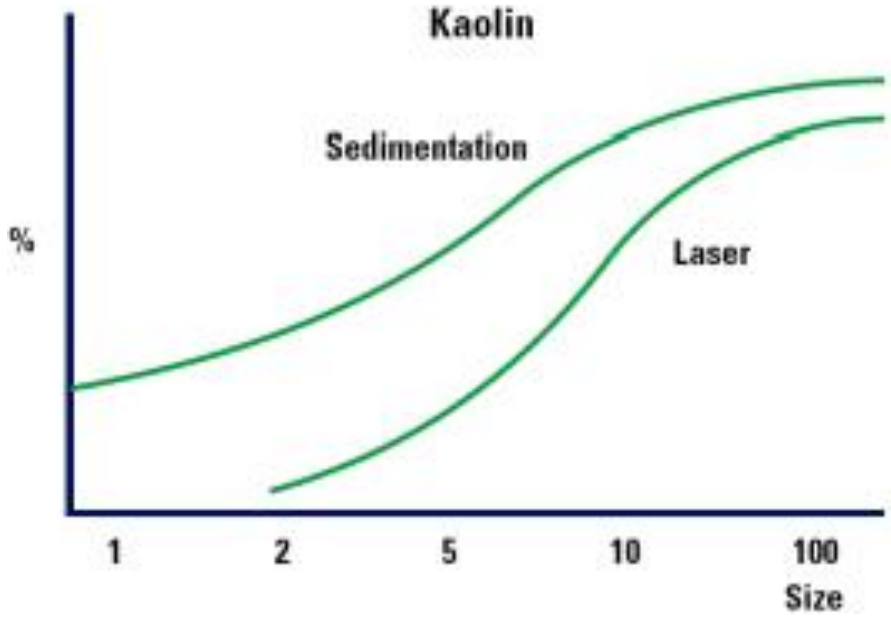

Figure 2. Expected difference in results obtained by sedimentation and laser methods

Conductometric method (electronic or Coulter method)

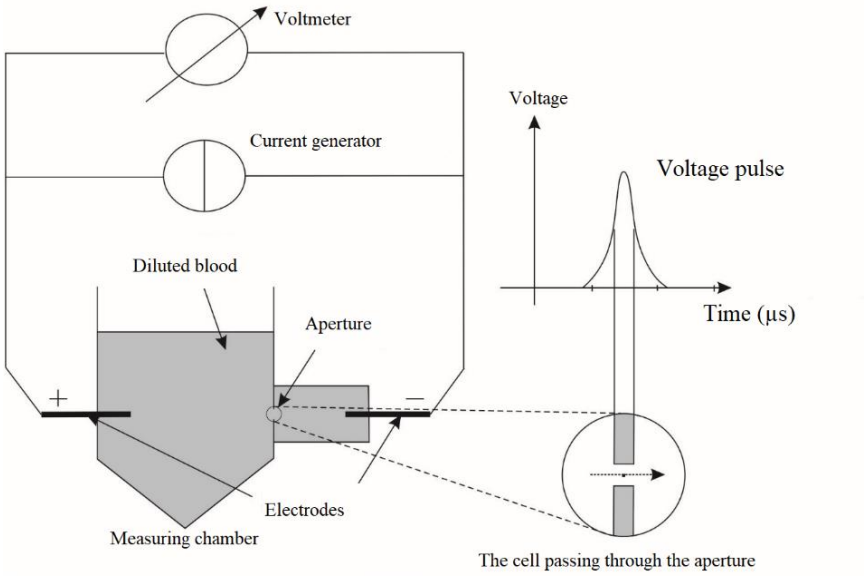

Figure 3. Schematic diagram of particle size measurement using the conductometric method

This analytical method was developed in the mid-1950s for the determination of blood cell size. The principle is as follows: a diluted suspension is passed through a calibration orifice in a glass vessel (tube) to which a potential difference is applied.

As the particles pass through the opening the capacitance changes stepwise, manifesting itself as a pulse or voltage peak. The height of the peak is compared to the peak height of a standard sample. The method is a comparative method requiring calibration.

By calculating the area under the peak instead of the peak height, corrections can be made for results related to the orientation of particles passing through the orifice.

The Coulter counter can easily measure particles from 0,2 μm in diameter up to 1 600 μm.

The most obvious advantages of this method are the detailed analysis of the particle size distribution as well as the fine size differentiation and the more accurate statistical analysis.

However the method has some limitations:

- it is difficult to analyse emulsions;
- it is not possible to analyse dry aerosols and powders directly;
- requires considerable time to analyse polydisperse samples, requires changing the calibration wells (to cover a wide size range), and can lead to clogging of the wells with large particles. Therefore the method is well suited for the study of blood cells but not for the analysis of particles of real materials.

Dynamic analysis

A range of analyzers is available which can make highly accurate measurements in the nano and sub-nano range from 0.5 nm to 200 nm. The induced lattice method is based on a new principle of measuring the size of nanoparticles for analysis. Specially arranged electrodes are placed in a medium containing dispersed particles, and an alternating voltage is applied to them. The result is a specific arrangement of the particles in the liquid, the so-called induced diffraction grating.

If the voltage is interrupted, the particles diffuse, and the diffraction lattice collapses. The transducer records the change in light intensity when the diffraction lattice collapses, thus providing data on the particle size distribution.

Microscopy

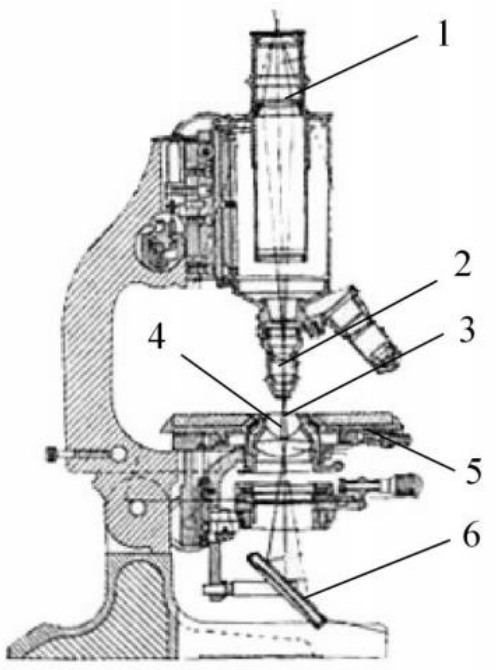

eyepiece (1), objective lens (2), test object (3), condenser (4),
objective stage (5), illuminating mirror (6)

Figure 4. Schematic View of an Optical Microscope

Microscopy is an ecellent analytical method to visualise particles and directly evaluate the degree of dispersion or agglomeration in a system. The main limitations of the method are its complexity, time of measurement, complexity of analysis, sufficient sample representativeness (large number of particles) and personal approach of the operator, in the case of electron microscopy the relative difficulty of sample preparation.

A package based on (automation), microscopy and image processing software can avoid subjectivity of the operator and provide extremely useful quantitative information when analysing a sufficient number of particles.

Investigation of the same sample by different operators can give completely different results. However, the combination of microscopy and laser diffraction certainly gives the most information about the sample.

Laser diffraction

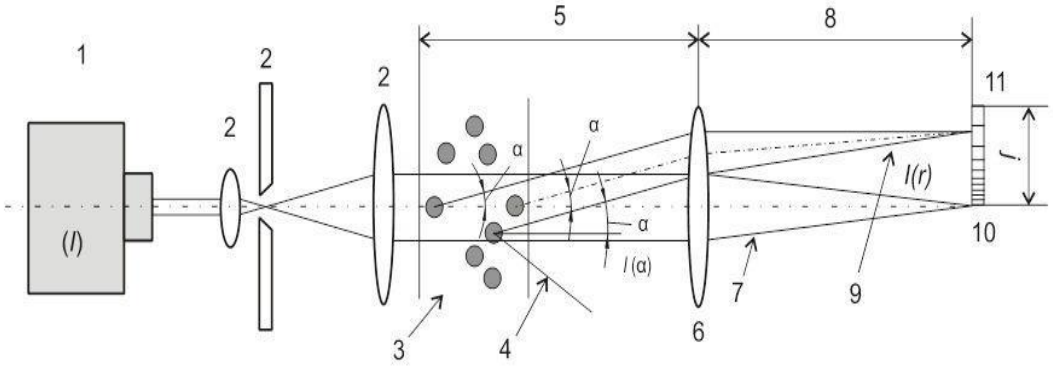

1 - Laser source, 2 - Laser processing module, 3 - Particles, 4 - Scattered light not collected by lens (6), 5 - Operating distance of lens (6), 6 - Fourier lens, 7 - Straight beam, 8 - Focal length of lens (6), 9 - Scattered beam, 10 - Dimming detector, 11 - Multi element detector

Figure 5. Schematic diagram of the Laser Diffraction Particle Sizer

Laser diffraction, also known as small angle laser light scattering (LALLS), has become the preferred method of particle size measurement in many industries, with ISO13320 defining 0.1-3000 μm as the testing range for this method. The method is based on the measurement of the intensity of scattered light, the angular dependence of which is determined by the particle size and its optical properties.

The analyser consists of the following main components:

1. Laser or coherent light source with a constant wavelength. HeNe gas lasers (=0.63 μm) offer the best performance in terms of signal stability and clarity.

2. Detectors. A multielement matrix of silicon photodiodes is typically used. Detectors with a good dynamic range, consisting of 32-44 elements, provide the best resolution, while increasing the number of elements has not been shown to improve actual resolution Basics of particle size analysis

Thus, the following advantages of the laser diffraction method can be noted.

- The method is based on fundamental principles.
- Calibration of the instrument, made in accordance with ISO 13320 in design, is not required.

- You can verify the operation of the analyser only by measuring a standard sample (verification).
- Wide dynamic range. It is capable of measuring particle sizes in the range from 0.1 μm to 2000 μm.
- Smaller particles (1 nm to 1 μm) are analysed by dynamic light scattering (photon correlation spectroscopy) and the results are objective as long as chaotic Brownian motion predominates in the system and no particles settle out.
- Universality. Capable of analyzing suspensions, emulsions, dry powders, aerosols and sprays
- Direct measurement of the particle size distribution of dry powders is possible, but not every system will provide high quality dispersion. In addition to suspension analysis, the results are informative for estimating the amount of agglomerated material in the dry phase.
- The particle size of suspensions and emulsions is measured by cycling the sample through the measuring cell, making the results highly reproducible and allowing the use of dispersant additives and surfactants to optimise dispersion.
- The analysis is performed on the entire sample. Although the amount of material required for the analysis is small (typically 4-10 grams for dry measurements and 1-2 grams for wet measurements) all material is passed through the laser beam and the contribution of each particle is considered. Considering the volume of the sample to be analysed, particular attention must be paid to the representativeness of the sample [1].
-

1.3.2 Conclusion of the review of methods for particle size determination

Among the existing laboratory and field instruments for determining particle size distribution there are none which are suitable for determining the particle size distribution in the feed cup of the thickener. As it was said before laboratory studies are not suitable because of breakdown of particles, and existing installations, such as installation for continuous automatic measurement of particle size distribution in pulp flow "PIK-074P", where the probe is mounted directly in the working environment, would disturb the process [2]. If such sensors and air supply to the probe and the inner wall of the feeder cup are installed, the integrity of the unit and, accordingly, the process of flocculation of pulp will be disturbed.

Scientific research on particle aggregation and coagulation was carried out at St. Petersburg Polytechnic University. The verification of particle sizes was carried out on the basis of photos of floccules obtained in the laboratory. In this case also it is not possible to claim about high quality of determination of sizes as in laboratory conditions it is difficult to maintain temperature of temperature control unit and layers of isolation prevent from getting accurate images to sensors. Also, one should not forget about the wall effect and the inconsistency in size of the particles adhered to the flocculus.

It is possible to solve the problem of particle size determination without direct interference with the process by using a virtual instrument based on the red mud slurry flocculation algorithm under development.

1.4 International and national experiences of the problem

1.4.1 The digitalisation of production

The use of digital systems, in particular digital twins and virtual instruments in process control, helps to improve process efficiency by implementing predictive control. Based on predictive control, potential risks can further be identified, new technologies can be integrated into existing production lines and project times and costs can be reduced. Modern technology makes it possible to build digital twins of absolutely any plant in metallurgical and refinery plants if sufficient process data are available. There is also a growing trend in the collection of synthetic process parameter data for machine learning of predictive control systems [3], [4].

Research is underway at the St Petersburg Mining University to develop an integrated digital automatic control system based on an adaptive state model for high-temperature and chemically aggressive media, using the digital twin model. This digital twin model can be used to control a complex process (aluminium electrolysis) in real time, to predict accidents and deviations in metallurgical production, to increase the current yield [5].

Virtual instruments can fully replace traditional measuring instruments (oscilloscopes, voltmeters, spectrum analysers, etc.). An important feature of the virtual instrument is that the software-generated and display-shaped front panel of the instrument can fully replicate the panel of a traditional measuring device [6].

1.4.2 Application of the PBE model in technology

The population balance equation (PBE) is the most used method for modelling particle aggregation, coagulation and flocculation. Foreign researchers use PBE to model particle aggregation by coagulants to further optimise the process and improve thickener design [7], [8]. Russian researchers in the field of mineral processing also use population balance equation to calculate flocculus size distribution as a function of time in coal preparation process [9].

PBE involves complete particle mixing, which needs to be incorporated into existing CFD models of the thickening process. Flocculation, which can be described by PBE, is the first step in the thickening process. Researchers prefer to study thickening in the free and settling zones to simplify the model. Duenas Diez (2004) discussed an additional advantage of the population balance model: "Creating a systematic strategy for developing PBE models that are both realistic for industrial plants and mathematically simple for online applications is the first step towards a wider use of PBE models in industry"[10].

1.4 Conclusion

In the first chapter of the master's work - state of the art the existing laboratory methods of particle sizing were studied. Unfortunately, these methods are not suitable for real-time sizing, indicating the need for virtual instruments.

During the review of existing solutions to the problem of implementation of digital systems in international and domestic experience was confirmed the relevance of implementing new systems in automated process control systems, especially in the metallurgical industry.

2. THEORY PART

2.1 General description of the process

Alumina production using the wet alkaline Bayer process is currently the dominant process in the global aluminium industry. The Bayer method is a leaching process designed to dissolve the Al2O3 alumina contained in the bauxite and to avoid the transfer of other bauxite components (SiO2, Fe2O3, etc.) into the solution. The method is based on a reversible chemical reaction.

$$Al2O3 - n\ H2O + 2NaOH = Na2O - Al2O3 + (n + 1)H2O.$$

When the reaction proceeds to the right, alumina in the form of sodium aluminate passes into solution, and when the reaction is reversed, hydrated Al2O3 precipitates out.

The list of basic operations of the Bayer method includes:

1. Preparation of the bauxite for leaching. Bauxite is crushed and ground to a fraction of 0.05-0.15 mm in a medium of added alkali and NaON recycled alkali solution, and a small amount of lime is also used as an additive to activate the leaching.

2. Leaching. The crushed pulp is sent to the next stage of production, leaching, according to the process flow sheet. The leaching reaction is considered to be completed by the formation of sodium aluminate.

To complete the reaction the following conditions must be met: high pressure (about 3 MPa), an alkaline environment, heating of the slurry to 100-240°C (depending on the bauxite grade) and its prolonged (about 2 h) stirring. The slurry is prepared in autoclaves - pressure vessels. The autoclave is designed as a steel cylindrical vessel with a height of 13.5-17.5m and a diameter of 1.6-2.5m. The pressure in the autoclave is 2,5-3,3 MPa, the pulp is fed from the top, and steam from the The slurry is pressed from above and steam is injected from below via a spigot with a barboter that heats and mixes the slurry. The slurry is pressed out of the autoclave through a pipe.

3. After dilution of the slurry with water, the separation of the aluminate solution from the sludge occurs in a 15-50 m thickener (settling tank) where the sludge settles to the bottom and the settled aluminate solution is discharged from the top. It also passes through a filter and is directed to the next step - decomposition. The resulting red sludge (it is given a colour by Fe2O3 particles) is sent to landfill and contains, %.

Al2O3 12-18, SiO2 6-11, Fe2O3 44-50, CaO 8-13.

4. Decomposition or decomposition of the aluminate solution is carried out in order to precipitate aluminium from the solution in the form of Al2O3 - 3H2O, and for this purpose the leaching reaction given above runs to the left towards the formation of Al2O3 - 3H2O. In order to make this reaction take place on the left side, it is necessary to reduce the working pressure to atmospheric pressure, dilute and cool the solution, introduce inoculants (small aluminium hydroxide crystals) and stir the pulp for 50-90 hours to obtain sufficiently large Al2O3 -3H2O crystals.

5. The aluminium hydroxide crystals then have to be separated from the solution and the crystals sorted by size. The decomposed slurry is sent to the thickener, where the hydroxide is separated from the solution. The hydroxide obtained in the hydroxidifier is separated into a fine fraction (<40 μm particle size) which is used as borehole for decomposition and a fraction with particle size of 40-100 μm. The coarse fraction is washed, filtered and sent for calcination.

6. Calcination or dehydration of alumina takes place in a tubular rotary kiln lined with chamotte 2.5-5 diameters and 35-110 m long, heated with natural gas or fuel oil. The hydroxide is slowly introduced into the hot gas stream along the rotating drum, and its temperature rises from 200-300°C at the charging point to 1200°C near the burner at the discharge end of the drum. When the hydroxide is heated, the reaction occurs: Al2O3 - 3H2O = Al2O3 + 3H2O, ending at 900°C. The product is aluminium oxide Al2O3 (white powder).

The extraction of alumina by the method described by Bayer is quite high - around 87%. To produce 1 ton of alumina it requires 2.0 - 2.5 tons of bauxite, 70 - 90 kg NaOH, about 120 kg of lime, 7-9 tons of steam, 160-180 kg of fuel oil (in fuel equivalent) and about 280 kWh of electricity [10].

2.2 Description of the control object

Thickeners are used in continuous processes where liquid and solid are separated by sedimentation. Thickeners have three main purposes:

- Concentration, or increasing the density of the mixture of solids and liquids (initial suspension).

- Clarification, which is the removal of solids from the mixture.

- Hydroseparation, which removes a certain fraction of solids from the mixture.

In some cases thickeners extract valuable solids and in others they extract valuable liquids. Thickening technology was originally developed in the mining industry. Before the

development of the continuous thickener, batch gravity thickening was used. In these batch operations, the diluted feed was pumped continuously into the tank until the overflow was no longer clear. The feed was stopped and the tank was left at rest until the solids had settled. After a suitable settling time, the clear overflow was decanted and the compacted sludge was removed.

The centrifugal centrifugal light duty thickeners are manufactured in housing diameters ranging from 2.5 to 18 metres. The heart of the single deck centrifugal centrifugal light duty thickener is a cylindrical metal casing with a small cone at the bottom. The centre of the bottom of the radial thickener is fitted with a discharge cone to discharge the thickened material, and an annular discharge chute at the top.

On the axis of the cylindrical body of the thickener, at the level of the liquid surface, there is a slurry inlet and a central shaft drive with a lifting mechanism for the combing frame. The shaft is mounted in support bearings on a bridge truss above the thickener housing.

The combing frame of the radial thickener consists of four rakes with angled rakes to move the sludge towards the centre. The rake carries the bottom sludge layer to the discharge point and compacts the sludge by creating pathways in the compression zone which allow the trapped liquid to escape upwards. A rake frame is used to raise the rake above the sludge layer if solids are not removed from the thickener fast enough. It facilitates reliable and continuous operation by providing sufficient lift to lift the rake out of the compaction zone or heavy solids during an emergency condition of the thickener. Lifting devices allow the tine arms to rotate during lifting or lowering. Hydraulic lifting devices have replaced manual or motorised mechanical screw-type devices.

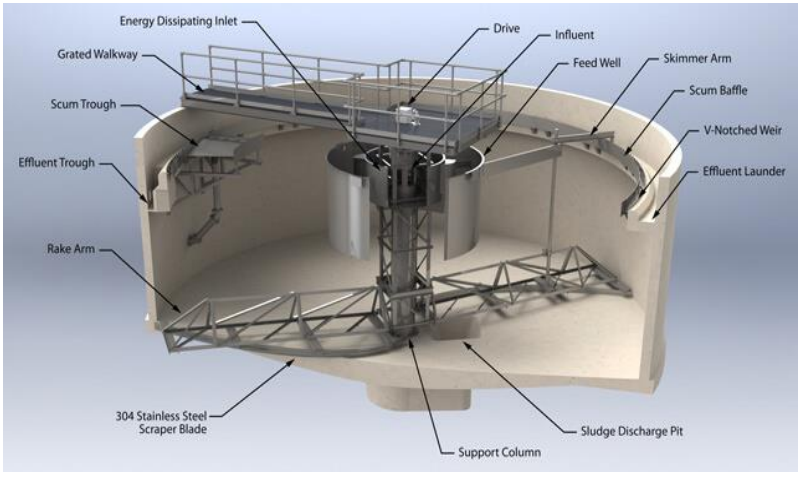

Figure 6. Radial Thickener

The feed slurry from the dilution agitator is fed into the plant through the feed line and into the lower part of the thickener zone - thickening and thickening. Due to the significant difference in slurry density, the thickening and thickening zone follows a different principle than conventional settling. For agglomeration and slurry formation, flocculants are added to a special thickening solution, thereby increasing the speed of the settling process and making it highly efficient. The raw material stream is rotated by means of rakes in a vat for thorough mixing with flocculant aid addition. The liquid phase is withdrawn from the thickened slurry and fed to the clarifying zone at the top of the thickener. The effluent is cleaner than in the traditional red sludge thickening method.

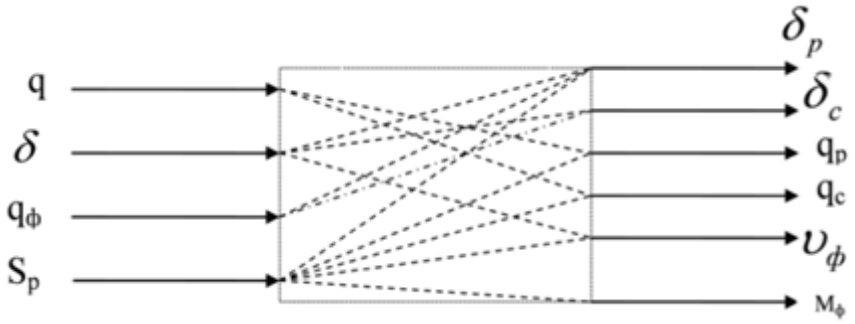

q - volume flow rate of pulp in the feed; δ - pulp density in the feed; qf - flocculant flow rate; Sp - discharging section area; p - discharge density; c - discharge turbidity; qr, qsl - volume flow rates of thickened product and thickener discharge; f , Mf - speed and momentum of thickener truss.

Figure 7. Input and output parameters of the thickening section

The more efficient the thickening plant, the higher the efficiency of the subsequent stages of alumina production. Stable operation of the concentration process depends on compliance with the following limitations

- The buffer tank must not be overfilled or emptied;

- Compliance with the specified criteria for the operating parameters of the processing plant;

- Compliance with the specified unit concentration rate;

- Compliance with the prescribed criteria for the chemical composition of the bauxite slurry.

This is justified by the fact that minor deviations from the prescribed technical scheme can lead to serious disturbances in the operation of the thickener, such as accidents or complete shutdowns.

The red mud sedimentation in the thickener produces the following zones:

1. clarified liquor discharge zone - cleared of red sludge particles and continuously removed from the apparatus;

2. the free settling zone is described by the empirical expression of Richardson and Zaki;

3. Constant and final concentration zone, with compression and thickening of the mud, with direct displacement of the aluminate solution

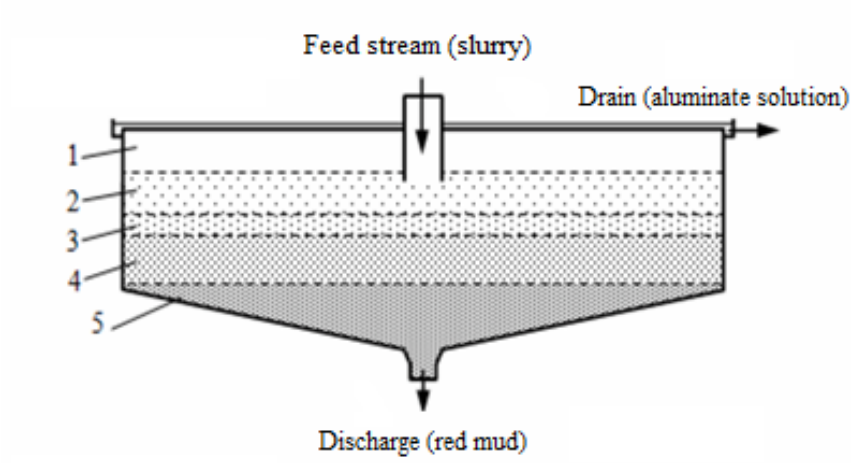

1 - clarified solution zone; 2 - free particle sedimentation zone; 3 - intermediate zone; 4 - compaction or compression zone; 5 - rowing action/solid compaction zone

Figure 8. Red mud thickening zones

In modeling of thickening unit often researchers, in order to simplify the model, disregard mixing of clarified solution and free particle sedimentation zone to simplify the description of the object. In real objects the particles from the free mixing zone under the action of velocity can rise above the feeder cup and fall into the clarified zone and further go through pipes to the discharge of purified aluminate solution [11].

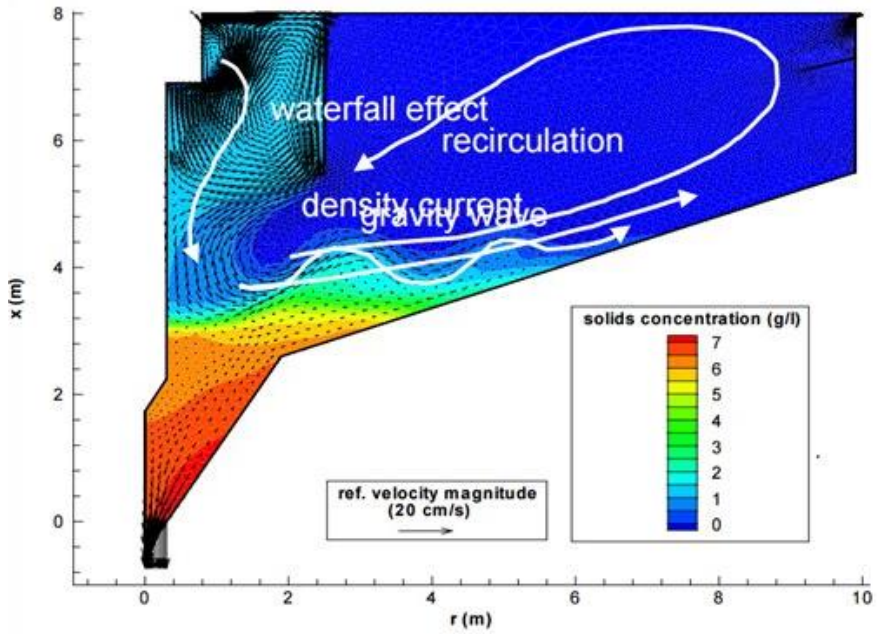

Figure 9. Velocity distribution of the substance in the thickener

2.3 Description and composition of RM

Red mud is a solid waste generated during the processing of bauxite, from which alumina is obtained. Bauxite is a mineral, a rock containing hydroxides and oxides of aluminium, iron, silicon and titanium.

The processing of bauxite produces red mud, which is discharged from the process as sludge (w:t=2-2.5) and dumped into sludge ponds. In Russia 2-3 tonnes of red mud is discharged for the production of 1 tonne of aluminium. Red sludge is a waste of human activity. A huge amount of waste - more than 100 million tons - has accumulated in the sludge dumps. The reservoirs cover a vast area (more than 100 hectares) and are a source of alkaline sludge water.

Red mud from different plants varies considerably in its phase composition. Frequently encountered minerals are hematite (present in quantity from 7 to 29 % practically in all slimes), goethite, bemite, gibbsite, anatase, rutile, ilmenite, perovskite, quartz, and also complex aluminosilicates of sodalite, cancrinite and kaolinite type. On average, the particle size of red muds is very small, varying from 100 nm to 200 μm.

Red mud contains up to 60 per cent metal oxides, mainly iron, which gives the waste its red colour. Red mud also contains significant amounts of silicon oxide, residual aluminium and titanium oxide. Red mud can also contain alkalis and heavy metals, the elevated levels of which pose an environmental threat.

It is known that full-scale processing of red mud began in 1982. The red mud was mixed with a lime constituent and then subjected to heat treatment at 1200 degrees Celsius in the presence of coke. The result is an iron-bearing product in the form of individual unbound particles, which are separated by magnetic separation, and sludge. The resulting sludge can be recycled.

The composition of the red mud varies depending on where the raw material comes from in the recycling plant. Typical composition, %. Al2O3 12-18, SiO2 6-11, Fe2O3 44 - 50, CaO 8 - 13.

2.4 Process parameters

The following process parameters have an effect on the thickening process: slurry pH and temperature, slurry density and shape, viscosity, mineral content, particle size distribution, solids content of the initial and thickened slurry, and the constructions of the thickening machines used.

Table 1. Process parameters for thickening.

Parameter under study	Units	Measuring range	Note
Process operating temperature	^oC	0-180	Controlled parameter
Volumetric flow rate of slurry in the thickener feed	m^3/h	0-1890	Disturbance parameter
Volume pumping speed of the thickened product	m^3/h	80-100	Control parameter
Concentration of solids in the feed slurry	% vol. frac	1.29 – 2.00	Measured parameter
Concentration of solid in the thickened bed	% vol. frac	2.83 – 6.00	Measured parameter
Concentration of flocculant solution	%	0.03-0.80	Measured parameter
Volumetric feed rate of flocculant solution	l/h	1200–1500	Control parameter
Dosage of flocculant	kg/t	0.1-0.20	Measured parameter
Solid phase density	kg/m^3	1400–1600	Controlled parameter
Liquid phase density	kg/m^3	0-400	Controlled parameter
Slurry viscosity at operating temperature 102^oC	Pa·s	0.0021	Controlled parameter

The efficiency of the concentration process is mainly determined by particle size: the larger the particles, the higher their settling rate. The particle coarsening of the slurry depends on the grinding conditions of the bauxite and its leaching behaviour. The need for coagulants and flocculants is due to the fact that the strong, heavily leached bauxite contains a high number of fine particles (1 to 10 μm) after grinding.

Today, an overwhelming number of manufacturers are switching to synthetic flocculants. At UAZ, Sytec HC-3000 flocculants are used in the thickening branch and the drainage rate has increased by a factor of 2 to 3.

Most of the red mud consists of particles smaller than 0.5 μm. Because the weight and size of the sludge particles are very small, they settle very slowly under gravity, and because it is also polydisperse, its particles settle at different rates: larger ones fall faster than smaller ones, and also collide with them more often. Thus, it can be concluded that in the presence of larger particles in the sludge the settling effect is better and the settling speed of the sludge is higher.

2.5 Flocculation kinetics

Coagulation and flocculation are the main processes in DS thickening. The sludge particles have the same electric charge in the aluminium salt solution and are repelled by the Coulomb force, preventing them from forming larger flakes. Due to the presence of coagulants during the thickening process, some of the particles of sludge with similar charges lose their charge and become electrically neutral. The thickness of the hydrate film on the particle surface rapidly decreases due to the presence of an electrical double layer. The formation of flakes is due to adhesive forces between the particles

Adsorption of organic heteropolarines on the particle surface causes disturbances in the stability of the flocculated suspension. During the process, conditions are created for adhesion forces between hydrocarbon units attached to the surface by flocculant molecules or ions and conditions are created for the formation of aggregates.

Various flocculant aid additives can influence the acceleration of the settling process. The dosing of flocculant aid can be varied by reducing or increasing the flocculant aid flow according to the amount of red sludge. Various synthetic flocculants are in active use at the moment: polyacrylamide, alkar, sedipur etc. Previously, rye meal and starch were ubiquitous in the metallurgical industry.

The switch to synthetic flocculants is based on a high deposition rate, which increases by a factor of 3 to 10 compared with the use of rye flour. Furthermore, the preparation, dosing and control process is fully automated. The consumption of these flocculants is an order of magnitude lower than that of flour.

The use of different flocculants and coagulants increases the capacity of the thickener and consequently the capacity of the red mud washing and thickening section.

The flocculation process is regarded as a sequence of the following steps:

- homogenisation of flocculant in the liquid phase of the suspension;
- Adsorption of flocculant on the particles of the solid phase;
- Flocculation itself, consisting in the formation of bridging bonds between particles;
- Growth of floccules (formation of aggregates of the 2nd and higher orders is also possible);
- Structural change of floccules;
- mechanical destruction;
- restoration of destroyed floccules.

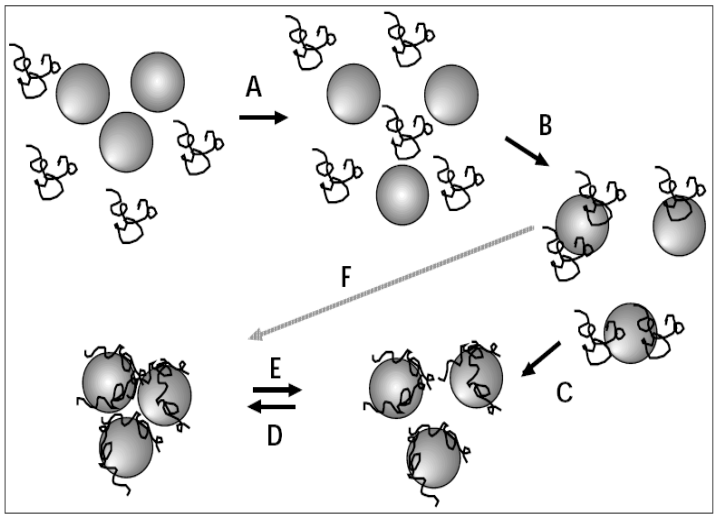

A - homogenisation of flocculant, B - adsorption of flocculant, C - change in flocculant molecules adsorbed, D - floc formation, E - flocculate degradation, F - flocculation without changing the conformation of the flocculant Flocculation, E - flocculate degradation, F - flocculation without change of conformation adsorbed macromolecules of flocculant

Figure 10. Schematic representation of the stages of the flocculation process

Regarding the kinetics of the process, there are two variants of the flocculation reaction:

- perikinetics - a characteristic feature of particles participating in Brownian motion in the dispersed phase (up to 1 micron thick);

- orthokinetics - for particles larger than 1 micron; the movement between particles and polymer macromolecules is mainly due to convective mass transfer.

Population equilibrium is currently the most commonly used method to describe flocculation kinetics. This model (Figure 11) takes into account the change in the number of aggregates of a given diameter and over time due to flocculation compaction and collapse.

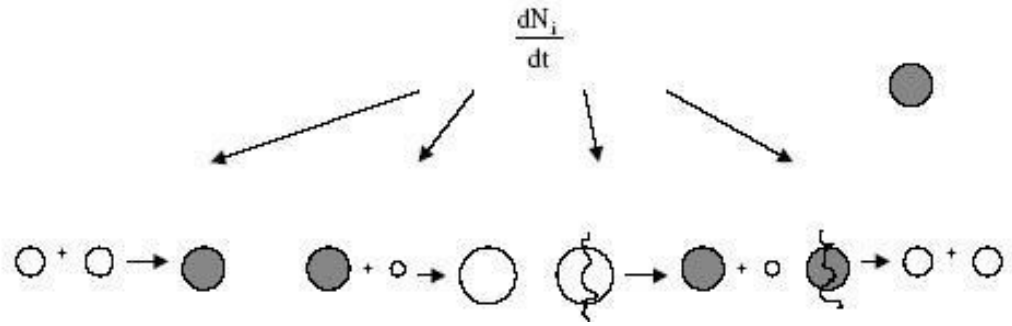

1 - formation of floccule of diameter i from two smaller floccules, 2 - exit of floccule from diameter i interval by aggregation with another floccule, 3 - formation of floccule of diameter i by destruction of the floccule of larger diameter, 4 - exit of the floccule from the range of diameter i by its destruction.

Figure 11. Schematic representation of the "population balance" model [12].

The population balance equation:

$$\frac{dN_j}{dt} = \sum_{j=1}^{i=2} 2^{j-i+1}\alpha_{i-1}\beta_{i-1,j}N_{i-1}N_j + \frac{1}{2}a_{i-1,i-1}\beta_{i-1,i-1}N^2{}_{i-1} - N_i\sum_{j=1}^{i=1} 2^{j-i}\alpha_{i,j}\beta_{i,j}N_j - N_i\sum_{j=1}^{max1}\alpha_{i,j}\beta_{i,j}N_j - S_iN_i + \sum_{j=1}^{max2}\Gamma_{i,j}S_jN_j \quad (2)$$

,where: N_i is the concentration of floccules containing 2_{i-1} particles; α_{ij} and β_{ij} are the collision efficiency and frequency of floccules of diameters i and j; S_i is the collapse intensity of floccules of diameter i; Γ_{ij} is the distribution function of collapse of floccules of diameter j to diameter i; max1 and max2 are the number of iterations.

2.5.1 Flocculus structure under static conditions

Information about the structure of floccules has been made available by a variety of investigations, such as sedimentography, laser diffraction, electron and atomic force microscopy (with digital imaging), laser diffraction, optical microscopy and computer simulations.

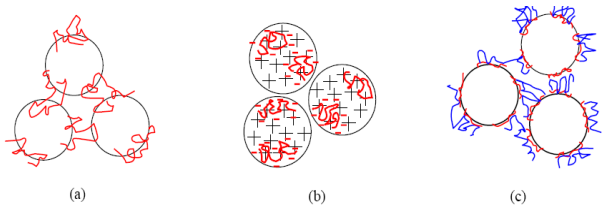

a - bridging flocculation; b - neutralising flocculation; c - flocculation with two polymers of different nature in series

Figure 12. Variants of flocculation structure [13]

Aggregates produced by the bridging mechanism are seen as a collection of particles bound together by polymer macromolecules; the space between the particles is filled with a dispersing medium.

The structure of perkinetic flocculants consisting of particles on the order of ten and one hundred nanometres, i.e. smaller than the size of the flocculant macromolecule, is less studied. The information available in several papers (e.g. [14];[15]) indicates that a single macromolecule can bind many particles, as shown in Figure 13.

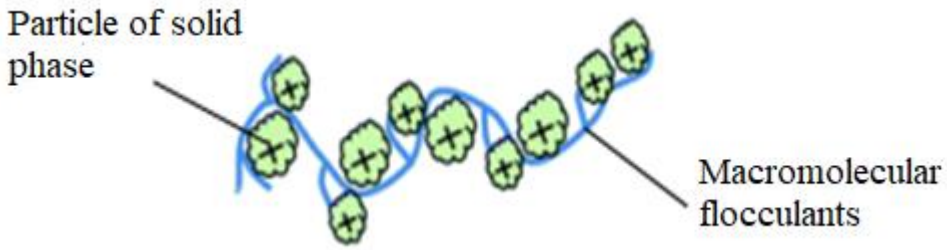

Figure 13. Structure of the bond between solids and flocculant

The geometric parameters of floccule are usually characterised by the mass fractal dimension DF. This value is determined by special methodology and characterises the degree of compactness of the flocculus. Depending on the shape of the aggregate, D_F can take values from 1 (linear structure) to 3 (sphere), as seen in Figure 14. The assumption of the fractal character of flocculation structures is also contained in [16]: the floccule is considered as a set of spherical particles of the same diameter, and the shape of the floccule

itself is also spherical (Figure 14). Along with D_F value, the parameter called "equivalent flocculus diameter" d_{EKB} is also used, which is numerically equal to diameter of the circle, the area of which is equal to the projection area of the flocculus.

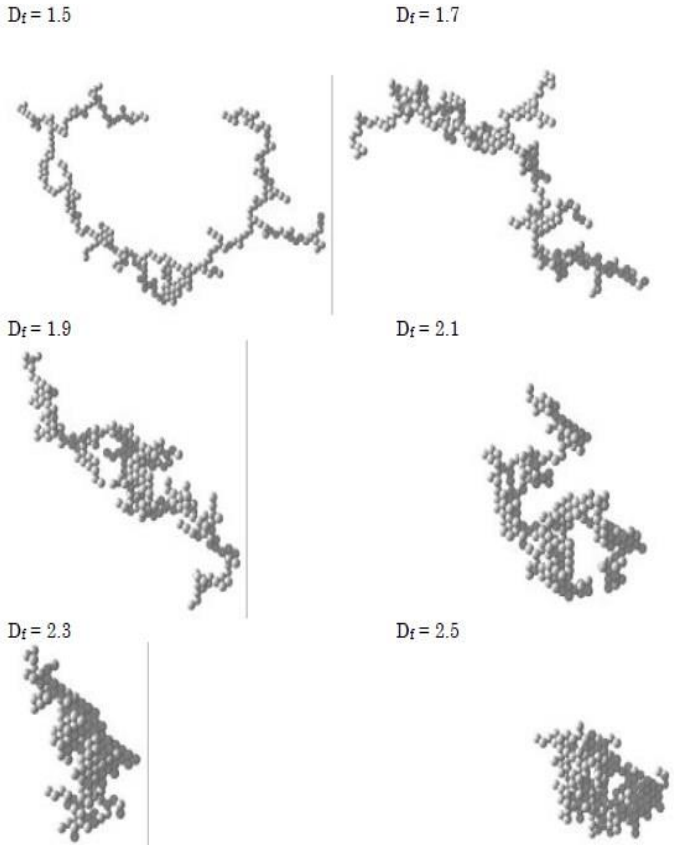

Figure 14. Units with different D_F values [17].

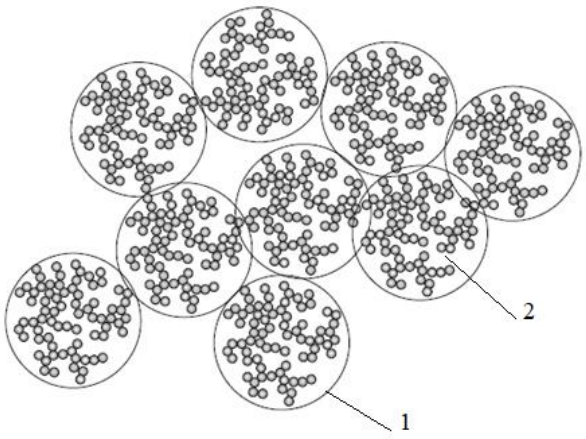

1 - flocculus; 2 - solid phase particle

Figure 15. Structure of floccules [18].

Orthokinetic flocculation of aggregates usually first forms loose and irregularly structured aggregates. Under certain conditions, the mutual arrangement of the individual parts of the floccules (clusters) changes, increasing the number of points of contact between them, resulting in aggregates becoming orderly and compact. In this process, the flocs aggregate into second-order aggregates several millimeters thick. This process is called "floc-granulation". Generally, when flocs are formed and subsequently compacted by mechanical synthesis, aggregates with a disordered structure are formed.

2.5.2 Parallel flow of floc formation and compaction

Two models have been proposed to describe the structure of the resulting aggregates.

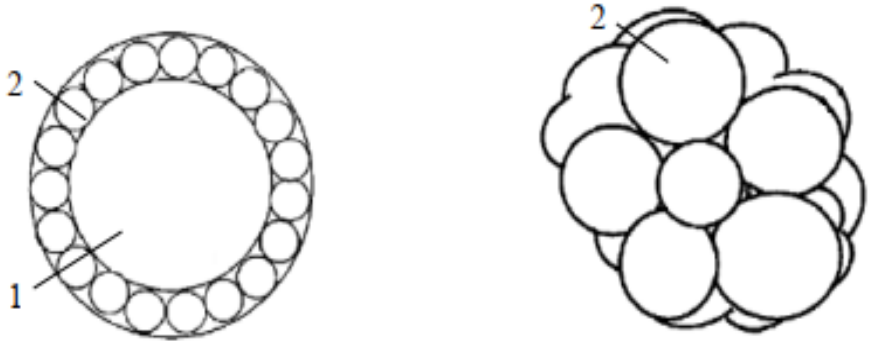

a - "bulbous" structure; b - "crimson" structure

1 - nucleus; 2 - first order flocculus

Figure 16. Schematic of the second order aggregates structure according to [19].

The second order aggregate of the "bulbous" structure, shaped like a sphere, consists of a nucleus and concentrically arranged layers consisting of individual particles or floccules. The core of the aggregate is a first order flocculus. It is possible to obtain a flocculus of "crimson" structure. This flocculus is assembled from first-order floccule, arranged in any order and shaped approximately spherical. The diameter of the flocculus can vary widely, from 100 nm to 1 mm.

The following parameters may influence the size of the aggregates:

- properties of the dispersion medium (pH, temperature, electrolyte concentration);
- the molecular weight of the flocculant; the mixing conditions of the suspension with the flocculant.
- the diameter, the shape, and the surface properties of the particles.

The following fact should be noted: the flocs formed by using two different flocculants in series can be larger in diameter than the flocs of the first order.

2.6 Population balance

The population balance equation (PBE) can describe the development of the population of small particles in a carrier fluid. PBE might be applied in carbon black modelling, reactive precipitation and coal combustion, aerosol technology, synthesis of nanoparticles, microbubbles. PBE is a transfer equation for the particle number density function. The particle number density function relies on spatial location, internal coordinates and time, which may include e.g. chemical composition, volume or surface area.

Mechanism of aggregate formation was described by Ahrens (2020):

"Growth: Particle growth occurs due to diffusion of dissolved substances on the surface, which thus expand. This process increases the internal properties, not the number of particles.

Decay: In the process of decay, large particles are broken up into two or more smaller fragments. In this case, the internal properties remain constant after growth, but the number of particles increases.

Nucleation: Nucleation is the process by which the smallest particles (most often dissolved in the ambient phase) precipitate out and form new particles. This increases the number of particles and gives an increase in the total sum of internal properties.

Aggregation: When two particles interfere, they have a chance to stick together and form stable bridging bonds in the area of contact. This process is called aggregation (or coagulation) and is the opposite of decay. It retains the sum of the internal properties but reduces the number of particles. As a consequence of these processes, the internal properties of the particles involved change over time, as does the total number of particles, making it difficult for a naive approach to track all particles individually" [20].

When particle collisions occur, the chances of aggregation rely primarily on the surface forces acting between the colloidal particles. Flocculation population balance equations usually incorporate kinetics, but largely ignore the surface and colloidal chemistry of the suspension. The equation is solved numerically as an initial value problem and is performed in time. In addition to the initial distribution, several larger channels (voids) are added. During flocculation, the particles in these channels migrate upwards.

Population equilibrium models require the initial particle size distribution of the source material as a starting point for modelling. However, in most cases the experimental size distribution cannot be used directly because population equilibrium has a certain internal interval between the size channels. This interval is coarser (fewer channels) than the interval defined by most modern particle measuring instruments and the initial equilibrium population size distribution can easily be obtained by interpolation.

A discrete version of the kinetic condensation equations was first proposed by the Polish scientist M. Smoluchowski when considering Brownian condensation in colloids. According to the original idea, it was true that the distribution system is spatially homogeneous. At time t=0 there are aggregates (particles) of different masses, which are multiples of particle masses.

Thus, an aggregate consists of particles, then its mass is $m_k=k_m m_0$. Under the influence of Brownian oscillations, the aggregates approach, collide and merge with a certain probability, creating new particles, whose masses are equal to the sum of the masses of colliding particles. Concentration of the disperse system is assumed to be unconcentrated for the convenience of investigating pairwise collisions. In this case triple or higher order collisions are not considered. To approximate the kinetic equation of Smoluchowski to the described model the weights of the equation will be changed.

2.7 Conclusion

In the second chapter of the master's thesis the technological course of the thickening process and its apparatus part were studied in detail. Separately the kinetics of flocculation was considered, where the formation of floccules, existing flocculants (synthetic and natural) were described in detail. Also, the population balance in terms of description of particle distribution in the liquid was described in detail.

3. EXPERIMENTAL PART

3.1 Laboratory experiment

The purpose of the experimental studies is to determine the geometric properties of the sphlocked red mud slurry after the deposition process in a temperature control unit at operating temperature**.**

Figure 17. Red mud sample from UAZ

Equipment:

- Thermostat - 1pc;
- Measuring cup 1l - 1pc;
- Measuring cup 0.5l - 1pc;
- 1 L volumetric flask - 1pc;
- 5 ml syringe - 2 pcs;
- 5 ml pipette - 1pc;
- Pipette 2 ml - 1pc;
- Slide Glasses - 4 pcs;
- Glasses - 4 pieces; Pears - 2 pcs;
- Thermometer - 1pc;
- Microscope - 1pc;
- Mixer - 1pc;
- Microscope camera - 1pc;
- Meter cylinder - 250 ml - 2pc;
- Distilled water for thermostat – 20 l;
- Rye flour - 0.5 kg.

Table 2. Preparation calculations.

Cylinder volume	250 ml
Slurry concentration	63,2 g/l
Volume fraction	2 %
Slurry quantity	250 ml
Mass of RM	15,8 g
Mass of flocculant aid	0,0158 g
Volume of flocculant solution concentration 0.5%	3,16 ml
Average flocculant aid consumption per 250 ml	2,37 ml

Process steps:

1) To carry out thermostating, assemble a temperature control unit consisting of a thermostat and an agitator. The working volume of the thermostat is filled with 25 liters of liquid (distilled water).

The unit consists of a heater, thermometer, thermostat, mixer and two 250 ml measuring cylinders. The mixer speed is set to 400 rpm.

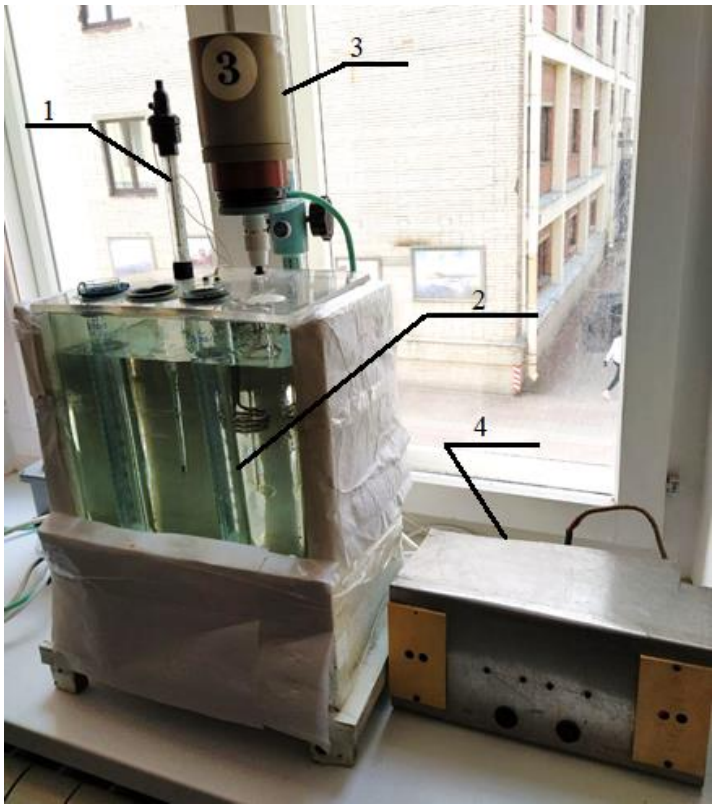

1 - Thermostat, 2 - 250 ml cylinder, 3 - Stirrer, 4 - Temperature control unit

Figure 18. Thermostat setting

The red sludge precipitation process takes place at a temperature close to the production thickening temperature of 90ºC.

2) A solution with a concentration of 63.2g/l was required to obtain the mixture under study. A sample of 63.2g of red mud was taken on measuring scales and diluted with distilled water to a volume of 1 litre.

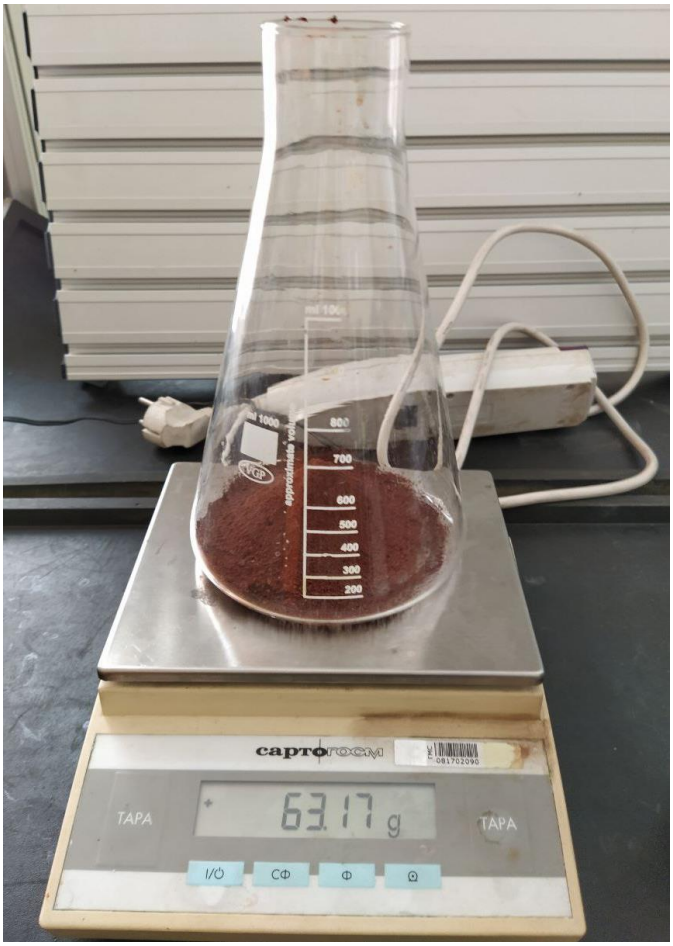

Figure 19. Sampling of RM

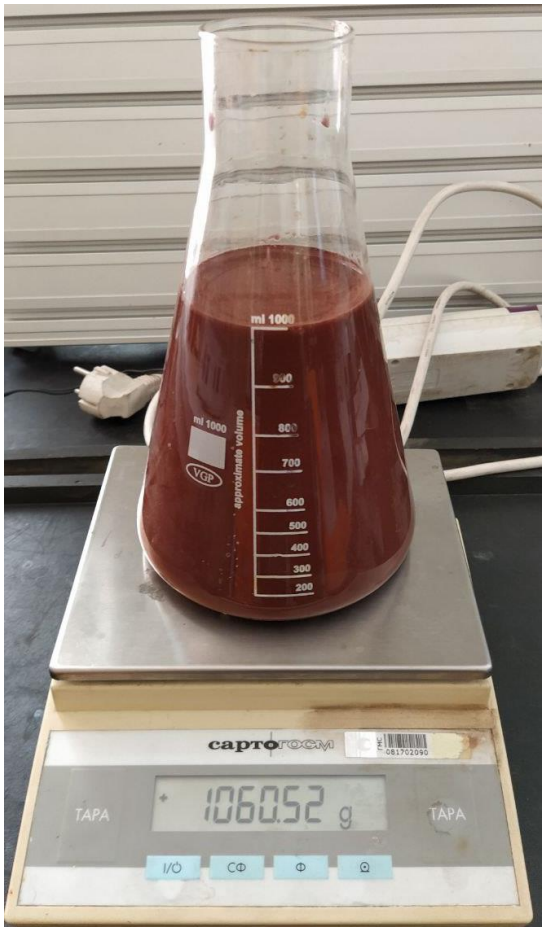

Figure 20. Preparing RM solution

3) About 2.5ml of flocculant was needed to sediment a 250ml sample of red mud solution. To obtain the flocculant, 0.25g of rye flour and 50ml of distilled water were mixed to obtain a solution with a concentration of 0.5%.

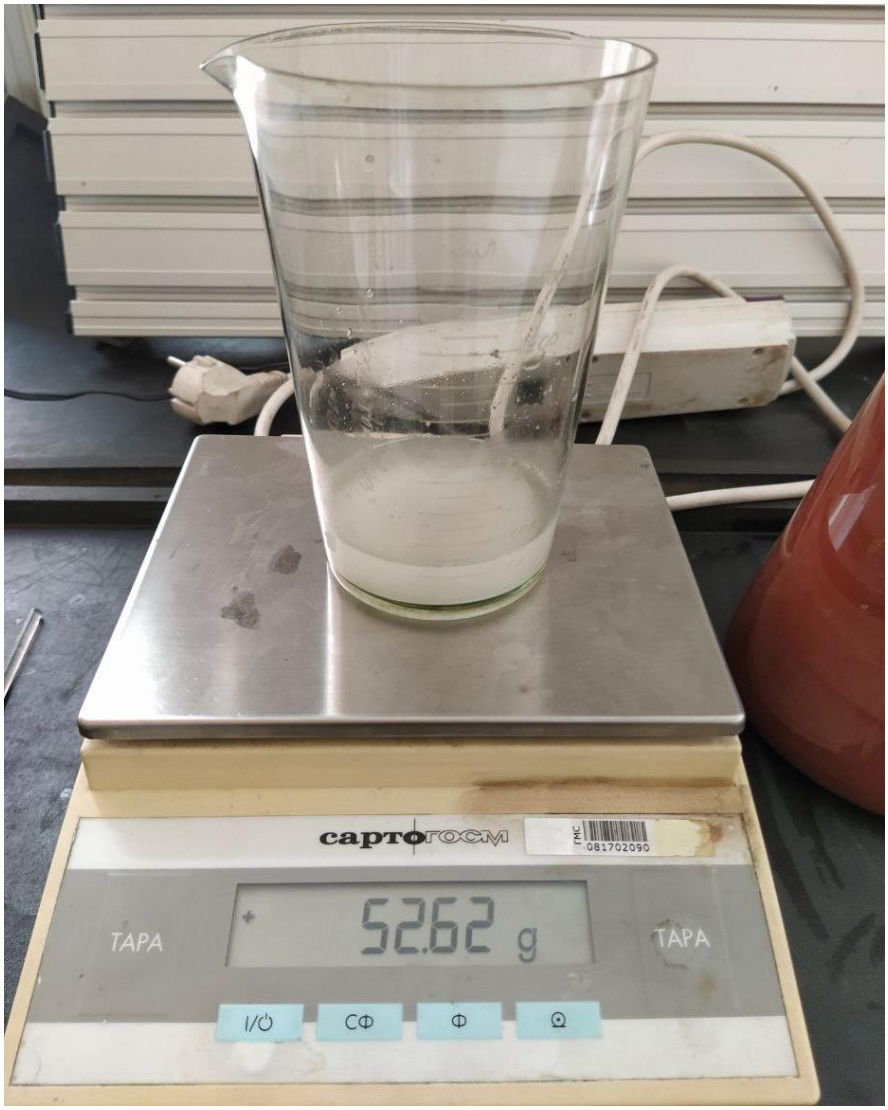

Figure 21. Obtaining a flocculant aid solution

4) When the thermostat reaches a temperature of 90°C, the tested RM slurry should be poured into measuring cups of 250ml placed inside the thermostat. The right measuring cup was filled with the test mixture one hour earlier than the second, but the dose of flocculant was added to both cups at the same time. In this way, the effect of the temperature of the medium on the settling velocity was investigated.

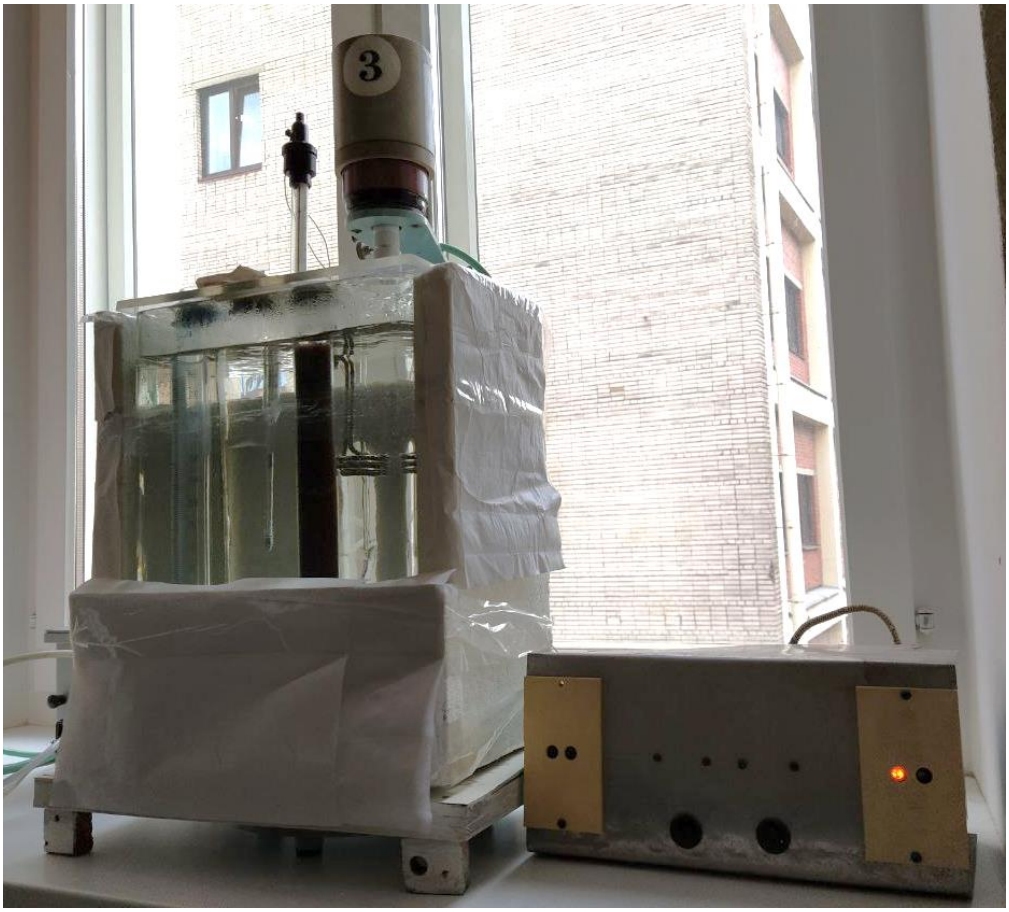

Figure 22. Operating the temperature control unit with the first RM slurry sample

During the first half hour, the test mixture in the first glass without the addition of flocculant aid partially precipitated by 5 mm.

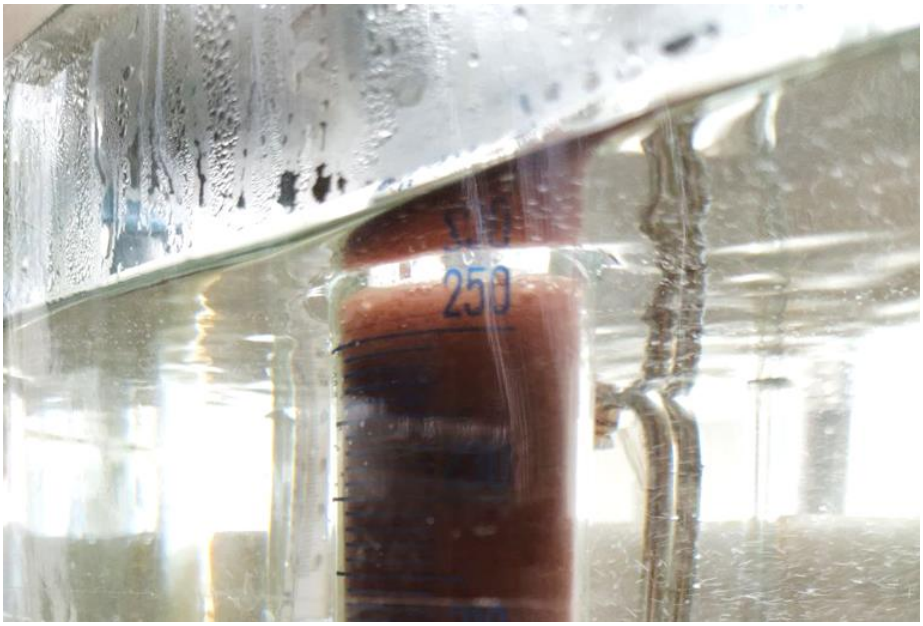

Figure 23. Initiation of RM slurry settling

After one hour the left measuring cup was filled and a dose of 2.5ml flocculant was added.

Figure 24. Temperature control unit with two filled measuring cylinders

The test mixture was left in the apparatus for 12 hours to assess the degree of RM sedimentation.

Figure 25. Degree of slurry deposition RM after 12 hours

From the results obtained, it can be concluded that settling in the heated medium was much better than in the medium in which flocculant aid was added immediately upon placement in the temperature control unit.

Then examine the settled material from the first sample under the microscope.

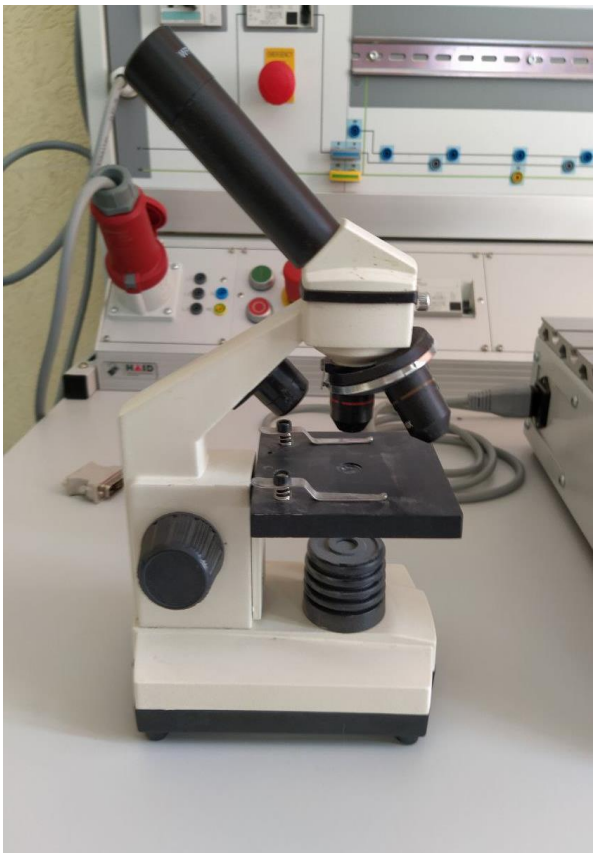

Figure 26. Microscope

Figure 27. Slides for the study of flocculated particles

When using the microscope, it was possible to magnify the illumination, change the colouring of the filters, zoom in/out the surface with the slide, and use 5x/10x/40x lenses.

Images of the sludge sample were taken with a HAYEAR microscope camera.

Figure 28. USB camera for microscope

In order to preserve the shape of the obtained sphlocked particles, the spent sludge sample was placed on a slide, not between panes.

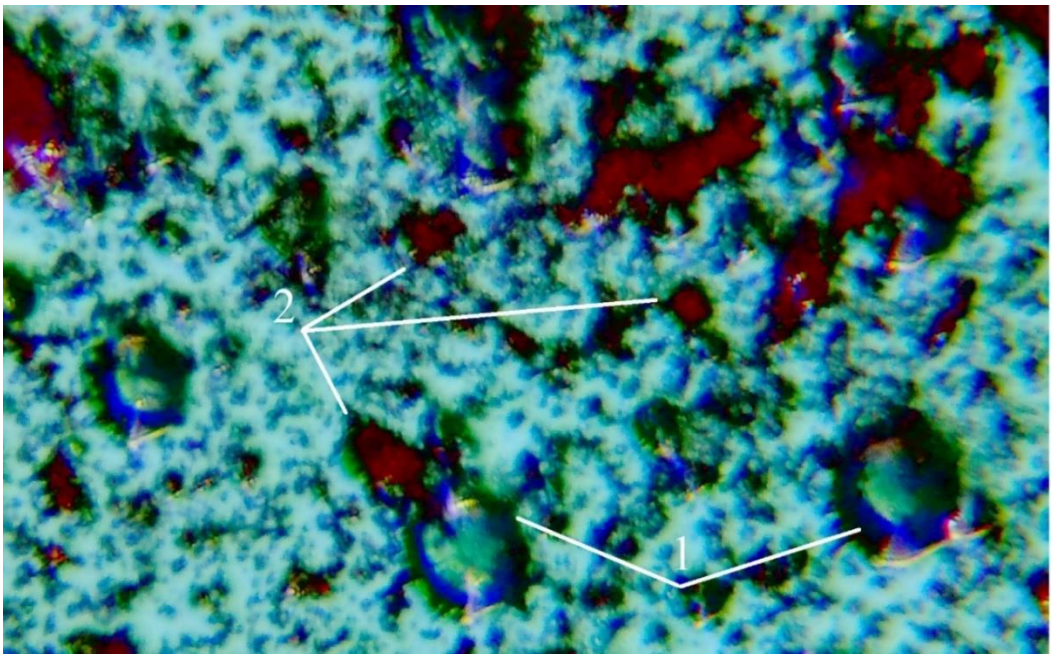

1 - Air bubbles, 2 - Flocculated particles of floculated RM

Figure 29. Sample of deposited RM with 10x magnification

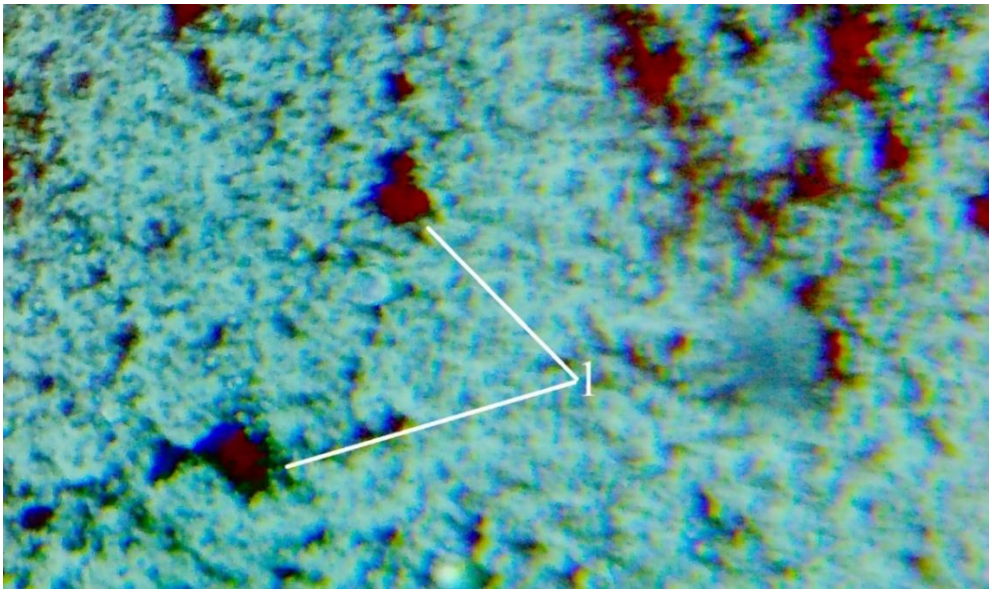

1- Flocculated particles of deposited media

Figure 30. Sample of deposited RM at 10x magnification

The accuracy of the experiment may have been disturbed by a number of factors:

- Process temperature;
- Suspension volume per work sample of RM slurry;
- The use of a non-synthetic flocculant aid.

There is therefore a high likelihood of large RM particles sedimenting instead of forming non-flocculated particles.

In the course of the experimental part of the master's thesis an experiment on RM pulp settling and flocculus formation was carried out. Rye flour was used as flocculant. The disadvantage of this type of flocculant is low speed of flocculation and hence low rate of sedimentation of RM particles. The temperature of carrying out of process differed from temperature of conducting process on manufacture on more than 15 ^{o}C because of the limited temperature limits of the laboratory equipment.

Also a significant factor in the slowing of deposition was the improper preparation of the RM sample upon arrival to the university laboratories. The brought sample due to high humidity and long storage without treatment formed large aggregates, due to which further splitting, drying and sieving reduced the fractional composition creating fine particles, which when mixed with water formed a hard to settle suspension. The sample had to be dried and sieved through a coarse sieve to preserve the original appearance of the RM coming from production as soon as it arrived in the laboratory.

4. PRACTICAL PART

As mentioned earlier the evolution of the population of small, i.e. non-inertial, particles in the carrier fluid can be described by the population balance equation (PBE). A population balance model needs the original size distribution of the feed stream particles as a starting point for modelling. However, in most cases the experimental size distribution cannot be used directly, as the population balance has its own defined channel spacing. This distance is coarser (if there are fewer channels) than specified by most current particle sizing instruments, in which case the initial population balance distribution can easily be obtained by interpolation. Currently, a simple linear interpolation is used in the Matlab model. If the experimental size distribution has only a few data points or the distribution is very noisy, a smoothed size distribution can be fitted first. The smoothed distribution is then used to interpolate to the original population balance distribution as before.

Each of the dimensional channels is described by an ordinary differential equation (ODE). Initially each channel will contain some number of particles (or no particles), which is determined by the initial distribution. After the addition of flocculant, the particles will start to form into aggregates, and the particles will disappear from the smaller channels and reappear as aggregates in the larger channels. The rate of loss or increase from each channel is determined by the aggregation and destruction kernels, where the kernel is a size dependent rate equation. The simulation is solved numerically by taking a series of small time steps and tracking the number of particles in each channel as the model moves through time.

A population balance model is essentially just a dynamic particle counting system.

PBE needs an initial particle size distribution. However, in most cases the experimental size distribution cannot be used directly due to the fact that the population balance model has its own channel size intervals (its own discretisation).

The population balance model is solved numerically as an initial value problem and unfolds in time. The starting point of the simulation is the particle size distribution of the raw material. Particles will migrate upwards into these channels during flocculation distribution.

The data obtained from UAZ RUSAL will be generated using the "normcdf" function built into Matlab, and subsequently modified to demonstrate the process of approximating the experimental distribution to a lognormal distribution.

The discretization of the population can be found in [21]. There is balance model described as follows:

$$\frac{V_i}{V_{i+1}} = 2 \tag{2}$$

where V_i is mass-equivalent volume of sinter in section i, i.e. volume of completely formed sinter which contains $x_i=2^{i-1}$ spherical monodisperse particles of diameter d_p:

$$V_i = \frac{\pi}{6} * d_i^3 = x_i v_p = x_i * \frac{\pi}{6} * d_p^3 \tag{3}$$

We define the minimum particle size as dp= 6.5e-6m, i.e. 6.5 μm. Use 39 channels in the population balance model.

$$V\_1 = \ 〚0{,}0000065〛\ \text{^}3 * 1 * \pi/6 = 1{,}4327\ \times\ 10\text{^}(-16)\ m\text{^}3$$

$$V\_2 = \ 〚0{,}0000065〛\ \text{^}3 * 2 * \pi/6 = 2.87441 \times\ 10\text{^}(-16)\ \text{m^3}$$

$$V\_3 = 〚0{,}0000065〛\text{^}3 * 4 * \pi/6 = 5.74882 \times\ 10\text{^}(-16)\ \text{m^3}$$

$$V\_4 = \ 〚0{,}0000065〛\ \text{^}3 * 8 * \pi/6 = 1.14976 \times\ 10\text{^}(-15)\ \text{m^3}$$

$$V\_5 = \ 〚0{,}0000065〛\ \text{^}3 * 16 * \pi/6 = 2.29953 \times\ 10\text{^}(-15)\ \text{m^3}$$

$$V\_6 = \ 〚0{,}0000065〛\ \text{^}3 * 32 * \pi/6 = 4.59905 \times\ 10\text{^}(-15)\ \text{m^3}$$

$$V\_7 = \ 〚0{,}0000065〛\ \text{^}3 * 64 * \pi/6 = 9.19811 \times\ 10\text{^}(-15)\ \text{m^3}$$

$$V\_8 = 〚0{,}0000065〛\text{^}3 * 128 * \pi/6 = 1.83962 \times\ 10\text{^}(-14)\ \text{m^3}$$

$$V\_9 = \ 〚0{,}0000065〛\ \text{^}3 * 256 * \pi/6 = 3.67924 \times\ 10\text{^}(-14)\ \text{m^3}$$

$$V\_10 = \ 〚0{,}0000065〛\ \text{^}3 * 512 * \pi/6 = 7.735849 \times\ 10\text{^}(-14)\ \text{m^3}$$

Let's generate the experimental data using the function "normcdf":

```
%% data generation
x=[1.43720416666667e-16,2.87440833333333e-16,5.74882E-16,
1.14976333333333e-15,2.29952666666667e-15,4.59905333333333E-15,...
9.19811e-15,1.83962e-14,3.67924e-14,7.35849E-13,1.4717e-13,
2.94339413333333e-13,5.88678826666667e-13,...
1.17735765333333e-12,2.35471530666667e-12,4.70943061333333e-12,
9.41886122666666e-12,1.88377224533333e-11,3.76754449066667e-
11,7.53508898133333e-11,1.50701779626667e-10,3.01404e-10,...
```

```
6.02807118506667e-10,1.20561e-09,2.41122847402667e-09,4.82245694805333e-
09,9.64491389610666e-09,1.92898277922133e-08,3.85796555844267e-
08,7.71593111688533e-08,1.54318622337707e-07];%задаем ось x
%%
%
l=normcdf(x,0.24*10^(-7),0.12*10^(-7));%generate a normal distribution for the given
values on the x-axis
experimdata=[x;l];
expdata=experimdata'; %transform
plot(x,l,'bo-',expdata(:,1),expdata(:,2),'m--'); % plot output
MaxFunEvals_Data=25000;
MaxIter_Data=2000;
TolFun_Data=5e-9;
TolX_Data=1e-20;
TolCon_Data=1e-19;
TypicalX_Data=[5*10^(-12),3*10^(-12)];
options=optset;
%set boundaries and primary values
x0(1)=0.4*10^(-12);
x0(2)=0.2*10^(-12);
lb(1)=7*10^(-16);
lb(2)=7*10^(-16);
ub(1)=0.0000001;
ub(2)=0.0000001;
% setting
options = optimset(options,'Display', 'iter');
options = optimset(options,'MaxFunEvals', MaxFunEvals_Data);
options = optimset(options,'MaxIter', MaxIter_Data);
options = optimset(options,'TolFun', TolFun_Data);
options = optimset(options,'TolX', TolX_Data);
options = optimset(options,'FunValCheck', 'on');
```

```
options = optimset(options,'PlotFcns', {  @optimplotx @optimplotfunccount
@optimplotfval @optimplotconstrviolation @optimplotstepsize @optimplotfirstorderopt
});
options = optimset(options,'Algorithm', 'active-set');
options = optimset(options,'Diagnostics', 'on');
options = optimset(options,'FinDiffType', 'central');
options = optimset(options,'TolCon', TolCon_Data);
options = optimset(options,'TypicalX', TypicalX_Data);
%минимизация функции
[x,fval,exitflag,output,lambda,grad,hessian] = ...
fmincon(@(w)iecost3(w),x0,[],[],[],[],lb,ub,[],options);
```

The code of the function itself for finding the minimum deviation:

```
function J=iecost3(w)
xx=w(1);% mat expectation
yy=w(2); %sqv'
%data load
load('experiment.mat');
X=expdata(:,1);
%first column as X value
Y(:,1)=expdata(:,2);
%assign to the first column Y the values from the array of experimental
%data(from the second column)
Y(:,2)=normcdf(X,xx,yy) %assign to the second column Y the HP values in points X from
the experimental data array
e=Y(:,1)-Y(:,2);% error
J=e'*e;%square error
end;
```

Now we need to get the values of this normal distribution at the sampling points of the population balance model.

```
load('koef.mat');
load('koef.mat');
nex=zeros(1,30);
nex(1)=0;
```

```
nex(2)=1.43720416666667e-16;
for i=3:1:31
   nex(i)=(nex(i-1)*2);
end
M=normcdf(nex,x(1),x(2));
MM=[nex(1:30)+diff(nex);diff(M)];
```

After changing the generated values, let us approximate the values to the normal particle distribution using the method of least squares:

The population balance model now needs to be transferred to Matlab. The population balance equation has the form:

$$\frac{dN_j}{dt} = \sum_{j=1}^{i=2} 2^{j-i+1}\alpha_{i-1}\beta_{i-1,j}N_{i-1}N_j + \frac{1}{2}a_{i-1,i-1}\beta_{i-1,i-1}N^2{}_{i-1} - N_i\sum_{j=1}^{i=1} 2^{j-i}\alpha_{i,j}\beta_{i,j}N_j - N_i\sum_{j=1}^{max1}\alpha_{i,j}\beta_{i,j}N_j - S_iN_i + \sum_{j=1}^{max2}\Gamma_{i,j}S_jN_j \quad (4)$$

The first two terms describe the formation of a floccule of diameter i from two smaller floccules. The next two terms describe the exit of the floccule from the diameter i interval by aggregation with other floccules. The fifth summand is responsible for the exit of the floccule from the diameter i interval.

A detailed calculation of the coefficients has been done by Barthelmes (2003):

”βi,j is the so-called collision kernel of particles and agglomerates. Collisions can be caused by shear of fluid layers or by the always present thermal motion. It can be assumed that thermal motion is negligible compared to shear only for particles smaller than a micron. For agglomerates:

$$\beta_{i,j} = 0.31 + Gv_p\left(x_i^{\frac{1}{D_f}} + x_j^{\frac{1}{D_f}}\right)^3 \quad (5)$$

,where G is the so-called shear rate, i.e. the spatial average velocity gradient, which is uniform and constant.”[21].

The shape of agglomerates is irregularly determined by voids, or vice versa, by the density of the agglomerate, which depends on the size of the agglomerate. It is possible to use the fractal dimension Df to describe particles as they appear to have fractal properties.

According to Barthemles ”in shear suspensions the fractal dimensionality is usually in the region of 2.1-2.7. Here the fractal dimensionality is constant, although it depends on G and the size of agglomerates.” [21].

Other needed koefficients were also found in Barthelmes’s (2003) work, such as collision diameter, kernel decay, mass - equivalent diameter, fragmentation parameter and so on:

”The collisional diameter of agglomerate section i refers to the number of primary particles xi with diameter d_p:

$$d_{c,i} = d_p x_i^{\frac{1}{D_f}} \quad (6).$$

The kernel of decay is the rate of particle breakdown and is related to the shear rate and size of agglomerates:

$$S_i = A' G^q V_i^{\frac{1}{3}} \quad (7)$$

, where Si is proportional to the mass-equivalent diameter:

$$d_i = V_i^{\frac{1}{3}} = x_i v_p^{\frac{1}{3}} \quad (8)” [21].$$

The fragmentation parameter A' and the degree q were determined experimentally. From the point in time when the agglomerates have already collapsed under the forces directed at them, G is replaced by the external shear stress of the slurry.

The characteristic shear stress τ is represented in dimensionless shear stress form. It is a measure of agglomerate strength: the greater τ is, the less susceptible the particles are to failure at a given shear stress:

$$S_i \propto \left(\frac{\eta G}{\tau}\right)^q \quad (9)$$

Barthelmes (2003) also highlighted the following property of shear stress: “The shear force acting on the collisional diameter of the particle, the mass equivalent diameter di is replaced by the collisional diameter in equation. However, agglomerates with the same collisional diameter but lower fractal dimension are more porous. They are much easier to

collapse under the action of shear forces because they contain fewer particle groups per unit volume and their strength is lower" [21].

"The linear dependence on the collisional diameter can be replaced by a power law, which shows that the fracture rate increases as the fractal dimension decreases, i.e. as the porosity of the agglomerates increases:

$$S_i \propto v_p^{\frac{1}{3}} \left(\frac{d_{c,i}}{d_p}\right)^{\frac{3}{D_f}} \quad (9)$$

According to a study by Pandey and Spielman (1982), who proposed:

$$S \propto V\text{^}m \quad (10)$$" [21].

"Where the value of degree m is experimentally determined (m=0.33). Since the porosity is independent of the size of the primary particles, the volume of primary particles differs from the relative size of the agglomerates. Let us combine all these transformations and substitute them in:

$$S_i = k_b \left(\frac{\eta \varphi_{tot} G}{\tau}\right)^q v_p^{\frac{1}{3}} \left(\frac{d_{c,i}}{d_p}\right)^{\frac{3}{D_f}} \quad (11)$$

For dilute suspensions ($\varphi \rightarrow 0$), where viscosity is a constant, for spherical particles (D_f=3), equation (10) is converted to equation (6)" [21].

The viscosity of suspensions with fractal-like agglomerates corresponds to suspensions with solid spheres with hydraulic diameters of agglomerates. There are different correlations between volumetric particle fractions and viscosity of suspensions. Barthelmes (2003) suggests using a one-parameter viscosity function:

"

$$\eta \varphi_{tot} = \frac{\eta_0}{\left(1 - \frac{\varphi_{tot}}{\varphi_m}\right)^2} \quad (12)$$

In this equation ϕ_{tot} is the effective or total volume concentration of the aggregates.

$$\varphi_{tot} = \sum_{i=1}^{i_{max}} N_i v_{c,i} \quad (13)$$

, where $v_{c,i} = \frac{\pi}{6} * d_c^3$ - the collisional volume of agglomerates. ϕt is the maximum volume concentration at which the viscosity tends to infinity, ranging from 0.58 to 0.67, where ϕt =0.6 is used as the average. The fragment distribution function Γi,j accounts for the fraction of fragments that change to size i when the agglomerate in section j breaks down" [21].

Assume only binary sinter fracture:

$$\Gamma_{i,j} = \begin{cases} 2, j = i + 1, \\ 0 \qquad else. \end{cases} \tag{14}$$

This subdivision into 2 roughly equal sized fragments is taken from photographic observations. ”The width of the agglomerate size distribution can be described by the numerical geometric ODEs or the volumetric geometric ODEs given by Hinds in 1999:

$$ln\sigma_{gn} = \left(\frac{\sum n_i \left(\ln d_i - \ln d_{gn} \right)^2}{\sum n_i} \right)^{\frac{1}{2}} \tag{15}$$

Where the geometric mean diameter is defined as:

$$lnd_{gn} = \frac{\sum n_i lnd_i}{\sum n_i} \tag{16}$$” [21].

The volumetric geometric standard deviation is obtained by replacing n_i by $V_i n_i$ in both equations by analogy. Sectional population balance model for maximum number of channels imax=39. The source code of the population balance model in Matlab syntax.

A system of 39 ODEs describing each of the sections:

```
function dNdt = odefunfik1(t,N)
dNdt = zeros(39,1); %% creation of zeros matrix
%%
%parameters for saving to a file
fid1=fopen('mem1.txt', 'a');
fid2=fopen('mem2.txt', 'a');
fid3=fopen('mem3.txt', 'a');
fid4=fopen('mem4.txt', 'a');
fid5=fopen('mem5.txt', 'a');
fid6=fopen('mem6.txt', 'a');
format=repmat('%f ',1,39);
format=['\n', format,','];
%%
%% area of the constant declaration
tzv=0.1; %% characteristic shear stress
kb=1;%dimensional equilibrium factor
G=0.1; %shear rate
nu0=10e-3; %viscosity
```

```
fit0=0.6; %maximum volumetric concentration of agglomerates at which viscosity tends to inf
q=1.3;%experimental value
ddd=6.5e-6;%-size of smallest primary particle
Df=2.35;%
%%
%% reference zone
a1=0;% zeroing 1 sum
a2=0;% zeroing 2 sum
a3=0;% zeroing 3 sum
a4=0;%zeroing 4 sum
fitot=0; %zeroing the sum to calculate slurry viscosity
%calculation of effective volume concentration of agglomerates
for=1:1:39
   dc=ddd*((2^(i-1))^(1/Df));%calculate collision diameter
   fitot=N(i)*(pi/6)*dc^3+fitot; % effective volume concentration of sinter
end
```

After declaring the constants and specifying the stochastic differential level, we proceed to solve the Smoluchowski equation. We start with the first differential equation:

```
%%
%first differential equation
%Calculate the fourth sum for the first DM
   for j=1:1:39
      dc(j)=ddd*((2^(j-1))^(1/Df));%% calculation of collision diameter
      vp=pi/6*ddd^3;% particle volume
      nutot=nu0/((1-fitot/fit0)^2);% one-parameter viscosity function
      fragkerns=kb*(nutot*G/tzv)^q*vp^(1/3)*(dc(j)/ddd)^(3/Df);%fragmentation kernel
      %fragmentation kernel distribution function of agglomerate fragments at the collapse of larger
      of a large sinter, it is assumed that the sinter breaks up into two
      equal size parts
      if j==2
         fragdistfun=2;
```

```
        else fragdistfun=0;
        end
        a4=fragdistfun*fragkerns*N(j)+a4;%calculate result
    end
%end of calculation of the fourth sum of DM
mem6(1)=a4;%write into array
%%
%calculate third sum for the first LU
for j=1:1:39
        bet(j)=0.31*G*pi/6*ddd*((2^(1-1))^(1/Df)+(2^(j-1))^(1/Df))^3;%collision kernel
        a3=bet(j)*N(j)+a3;
%calculate result
end
mem4(1)=a3*N(1);
% fragmentation kernel for the first DN does not exist, as the primary
% particles are assumed to be non-degradable
%%
% fifth term
dc=ddd*((2^(1-1))^(1/Df));% calculation of collision diameter
vp=pi/6*ddd^3;% particle volume
nutot=nu0/((1-fitot/fit0)^2);% one-parameter viscosity function
fragkerns=kb*(nutot*G/tzv)^q*vp^(1/3)*(dc/ddd)^(3/Df);%fragmentation kernel
mem5(1)=N(1)*fragkerns;
%%
dNdt(1)=mem6(1)-mem4(1)-mem5(1);
% end of the first DM
mem1(1)=0;%write to array
mem2(1)=0;%write to array
mem3(1)=0;%write to array
%write to array
a3=0;%zeroing 3 sum
a4=0;%zero 4 sum
%%
```

```
%Second Difference Equation
%Calculating the second sum of the second DDE
bet=0.31*G*pi/6*ddd*((2^(2-1))^(1/Df)+(2^(1-1))^(1/Df))^3;%collision kernel
a2=2^(1-2)*bet*N(1);%calculate result
%end of calculation of the second term
mem3(2)=a2*N(2);
%%
%% calculation of third sum for second DM
for j=2:1:39
      bet(j)=0.31*G*pi/6*ddd*((2^(2-1))^(1/Df)+(2^(j -1))^(1/Df))^3;%collision kernel
      a3=bet(j)*N(j)+a3;
end
% end of calculation of the result of the third sum for the second DU
mem4(2)=N(2)*a3;
%%
%% calculation of the fourth sum for the second LU
   for j=2:1:39
dc(j)=ddd*((2^(j-1))^(1/Df));% collision diameter calculation
      vp=pi/6*ddd^3;% particle volume
      nutot=nu0/((1-fitot/fit0)^2);% one-parameter viscosity function
      fragkerns(j)=kb*(nutot*G/tzv)^q*vp^(1/3)*(dc(j)/ddd)^(3/Df);%fragmentation kernel
      %fragmentation kernel distribution function of agglomerate fragments at the collapse
of larger
      of a large sinter, it is assumed that the sinter breaks up into two
      equal size parts
      if j==3
         fragdistfun=2;
      else fragdistfun=0;
      end
      a4=fragdistfun*fragkerns(j)*N(j)+a4;%calculate result
   end
%end calculation of the fourth sum for the second DM
mem6(2)=a4;
```

```
%%
% fifth term of the equation
  dc=ddd*((2^(2-1))^(1/Df));%% calculation of collision diameter
  vp=pi/6*ddd^3;% particle volume
  nutot=nu0/((1-fitot/fit0)^2);% one-parameter viscosity function
  fragkerns=kb*(nutot*G/tzv)^q*vp^(1/3)*(dc/ddd)^(3/Df);%fragmentation kernel
%fragmentation fifth term of the equation
mem5(2)=fragkerns*N(2);
%%
second term of the equation
bet=0.31*G*pi/6*ddd*((2^(1-1))^(1/Df)+(2^(1-1))^(1/Df))^3;
mem2(2)=(1/2)*bet*(N(1))^2;
%end of the second term of the equation
mem1(2)=0;
dNdt(2)=mem2(2)-mem3(2)-mem4(2)-mem5(2)+mem6(2);
%end of second DR
a2=0;%zeroing of 2nd sum
a3=0;%zero 3 sum
a4=0;%zero 4 sum
for i=3:1:20 %calculate first sum
   for j=1:1:i-2
      bet(j)=0.31*G*pi/6*ddd*((2^(i-2))^(1/Df)+(2^(j-1))^(1/Df))^3;%collision kernel
      a1=2^(j-i+1)*bet(j)*N(j)*N(i-1)+a1;%calculate result
   end
   mem1(i)=a1;%first term
   second term
   bet=0.31*G*pi/6*ddd*((2^((i-1)-1))^(1/Df)+(2^((i-1)-1))^(1/Df))^3;
   mem2(i)=(1/2)*bet*(N(i-1))^2;
%%
   %calculate second sum
   for j=1:1:i-1
      bet(j)=0.31*G*pi/6*ddd*((2^(i-1))^(1/Df)+(2^(j-1))^(1/Df))^3;%collision kernel
      a2=2^(j-i)*bet(j)*N(j)+a2;%calculate result
```

```
    end
    %third member
    mem3(i)=N(i)*a2;
%%
    %calculate third term
    for j=i:1:38
        bet(j)=0.31*G*pi/6*ddd*((2^(i-1))^(1/Df)+(2^(j-1))^(1/Df))^3;%collision kernel
        a3=bet(j)*N(j)+a3;%calculate result
    end
    %end third term
    %fourth term
    mem4(i)=a3*N(i);
    %fourth term
%%
    %% calculation of the fourth sum
    for j=i:1:38
        dc(j)=ddd*((2^(j-1))^(1/Df));% calculation of collision diameter
        nutot=nu0/((1-fitot/fit0)^2);%single parameter viscosity function
        fragkerns(j)=kb*(nutot*G/tzv)^q*vp^(1/3)*(dc(j)/ddd)^(3/Df);%fragmentation kernel
        %fragmentation kernel distribution function of agglomerate fragments at the collapse
of larger
        of a large sinter, it is assumed that the sinter breaks up into two
        identical parts
        if j==i+1
            fragdistfun=2;
        else fragdistfun=0;
        end
        a4=fragdistfun*fragkerns(j)*N(j)+a4;%calculate result
    end
%%
    %sixth member
    mem6(i)=a4;
%% fifth term of the equation
```

```
    dc(i)=ddd*((2^(i-1))^(1/Df)); %% calculation of collision diameter
    vp=pi/6*ddd^3;% particle volume
    nutot=nu0/((1-fitot/fit0)^2);% one-parameter viscosity function
    fragkerns(i)=kb*(nutot*G/tzv)^q*vp^(1/3)*(dc(i)/ddd)^(3/Df);%fragmentation kernel
    mem5(i)=fragkerns(i)*N(i);
    %end of the fifth term of the equation
    a1=0; a2=0; a3=0; a4=0;
    dNdt(i)=mem1(i)+mem2(i)-mem3(i)-mem4(i)-mem5(i)+mem6(i);
end
meme1=mem1';
meme2=mem2';;
meme3=mem3';;
meme4=mem4';
meme5=mem5';;
meme6=mem6';
count1=fprintf(fid1,format,meme1);
count2=fprint(fid2,format,meme2);
count3=fprint(fid3,format,meme3);
count4=fprint(fid4,format,meme4);
count5=fprint(fid5,format,meme5);
count6=fprint(fid6,format,meme6);
fclose(fid1);
fclose(fid2);
fclose(fid3);
fclose(fid4);
fclose(fid5);
fclose(fid6);
end
```

Each member of each DM is written separately to a special file for further comparison. The source code of the file for solving the DU and displaying the results:

```
load('lastresult.mat')
Gr=MM(2,:);
[t,N] = ode15s(@odefunfik1,0:100,Gr);
```

```
GG=MM(1,:);
 hold on
for i=1:100
  plot(1:39,N(i,:));
  pause(0.01);
end
```

To visualise the work, an interface has been created that allows the PBE solution to be adjusted and the results visualised.

The first screen consists of a setting field for the PBE calculation and a cumulative distribution graph. The main parameters that can be changed during the calculation are listed below.

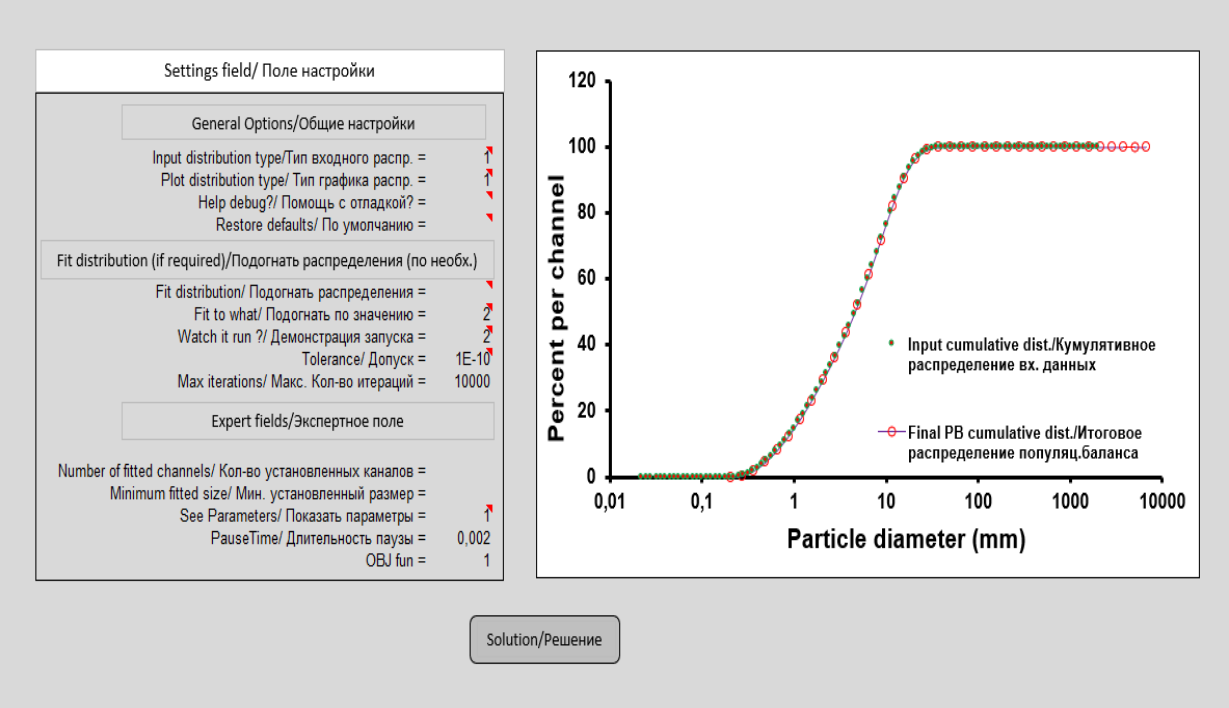

Figure 31. Population balance calculation parameter settings window

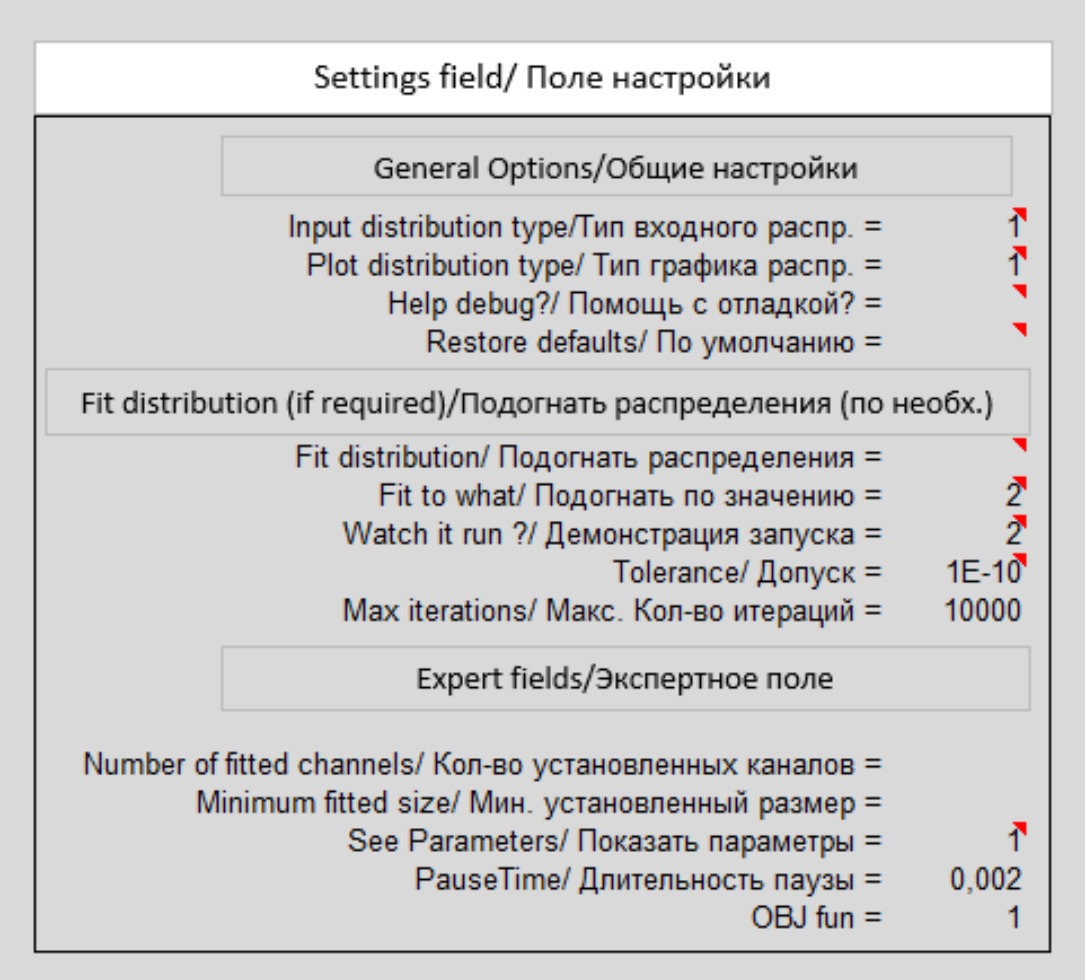

Figure 32. Setting field

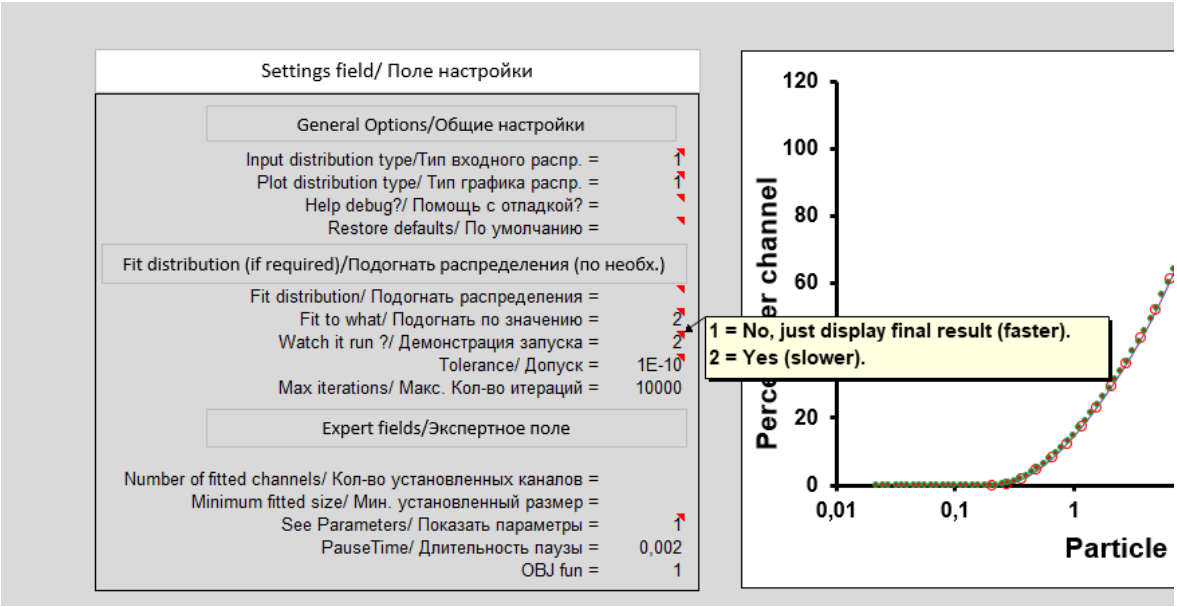

Figure 33. Selecting options in the fields

Table 3. Description of options in the settings field.

Parameter	Options
Input distribution type	1. Lognormal bell-shaped distribution 2. Cumulative Pass-Through Percentage Distribution 3. Omyacarb-1 Calcite 4. Omyacarb-2 Calcite 5. Omyacarb-5 Calcite 6. Omyacarb-10 Calcite 7. Omyacarb-20 Calcite 8. Kaolin 9. Example of a noisy cumulative distribution 10. Example of screening distribution
Plot distribution type	1. Lognormal "bell-shaped" distribution 2. Cumulative distribution of the pass percentage 3. Both
Help debug?	1. True
Restore defaults	1. True
Fit distribution	1. Yes, fit a simple distribution to the data points. 2. Yes, but fit two overlapping distributions
Fit to what	1.Fit a lognormal "bell-shaped" distribution 2. Fit a cumulative pass percentage distribution
Watch it run?	1. No, only demonstration of the final result, (quick) 2. Yes, (slowly)
See Parameters	1. Yes 2. Yes and initial approximation of the input values

Click the "Solution" button to go to the "PB Solution" window. This window allows you to change the calculation and calculation coefficients, as well as to change the appearance of the graphs and their layout.

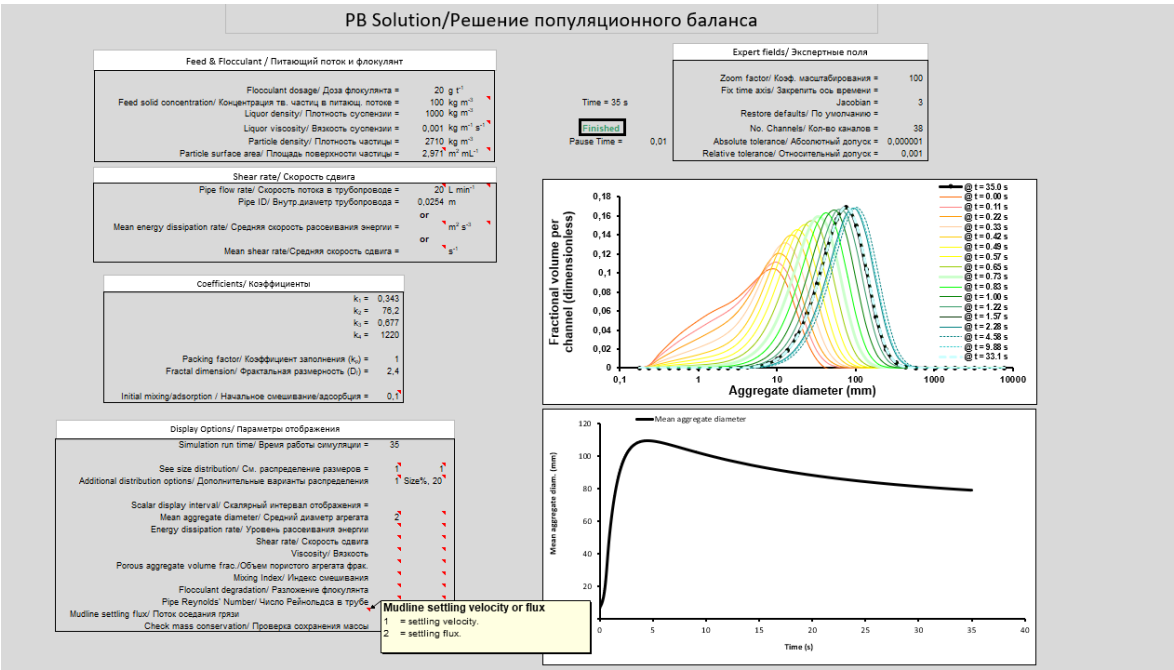

Figure 34. Population analysis solution window

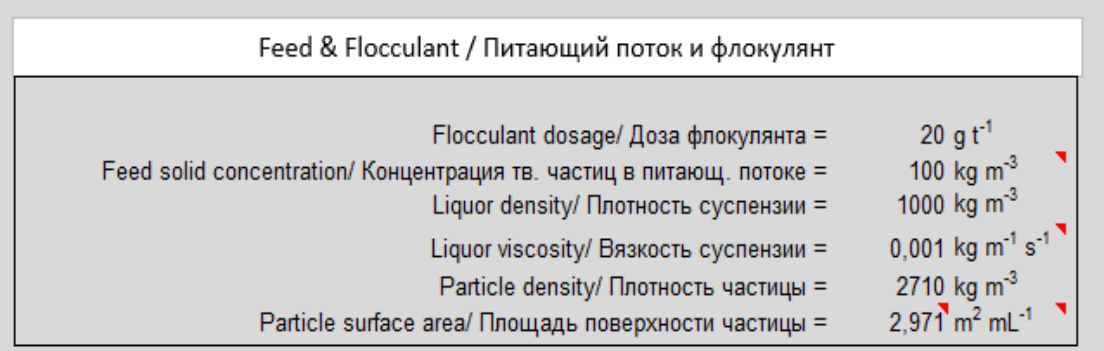

Figure 35. Feed flow and flocculant setting field

Table 4. Feed flow and flocculant setting field options.

Parameter	Notes	Unit selection option
Feed solid concentration	-	1. $kg*m^{-3}$; 2. wt%; 3. объемная доля, m^3m^{-3}(безразмерная).
Liquor viscosity	The parameter is calculated and entered automatically	1. m^2*m/L; 2. m^2/g.

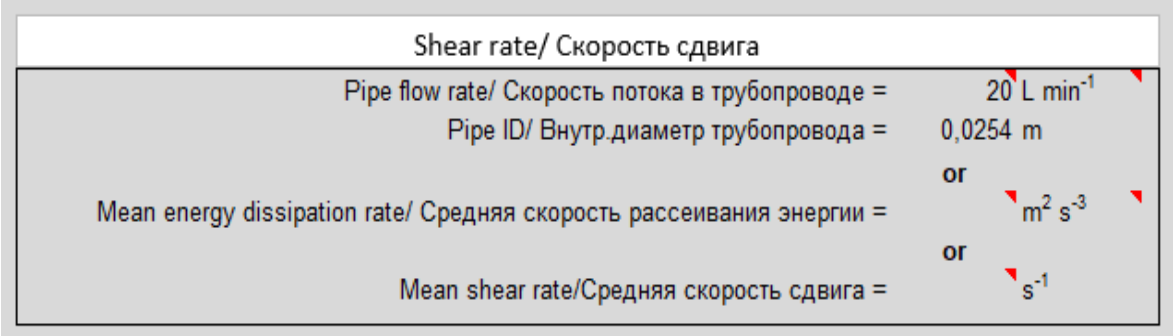

Figure 36. Shear rate setting field

Table 5. Description of options in the shear rate field

Parameter	Notes	Unit selection option
Pipe flow rate	When entering the value in the simulation, it is taken into account that the flow passes through the pipe space	1. m^3/s; 2. L/min; 3. m/s
Mean energy dissipation rate	When entering a value in the simulation, the energy dissipation rate is taken into account	1. m^2/s^3 2. J/s*kg
Mean shear rate	When entering a value in the simulation, the mean shear rate is taken into account	-

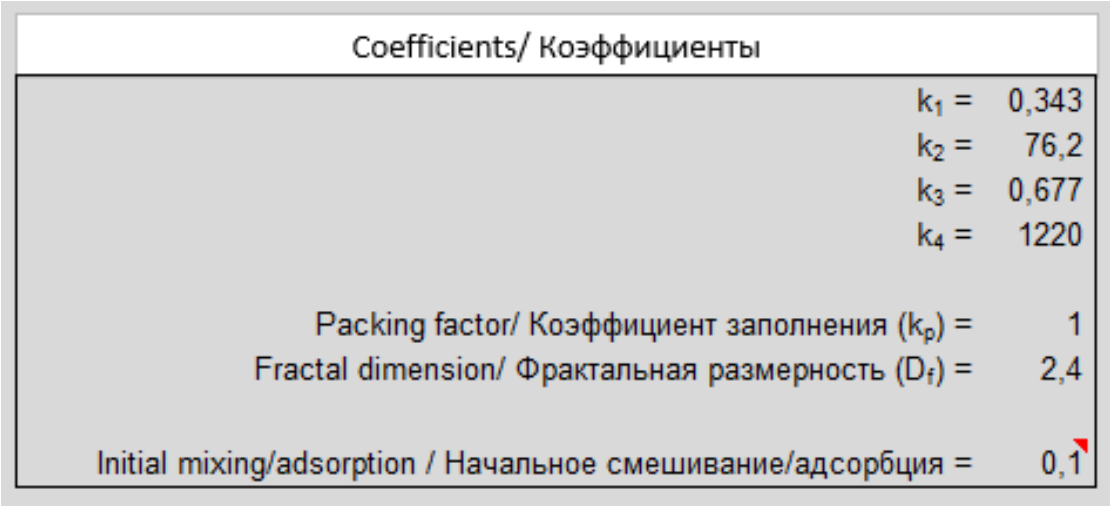

Figure 37. Coefficient entry fields for population balance solution

Table 6. Description of notes in the coefficient entry field.

Parameter	Note
Initial mixing/adsorption	A value can be entered to account for when the flocculant solution is introduced into the feed slurry

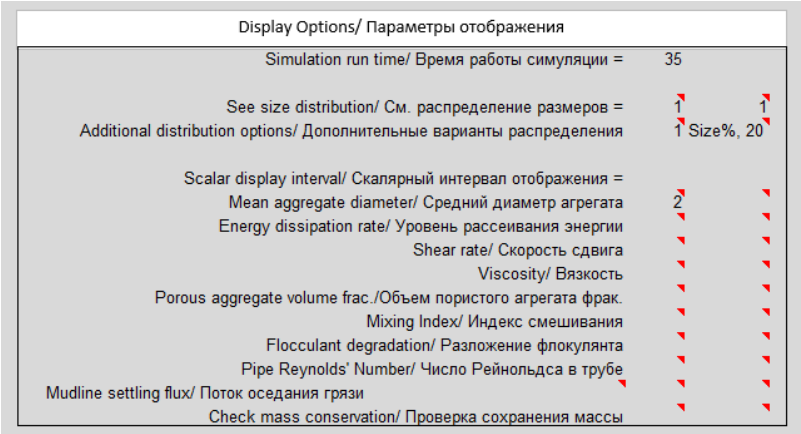

Figure 38. Display options

Table 7. Description of the option windows of the display options field.

Parameter	Option box 1	Option box 2
See size distribution	1. Yes, at each time step of the solver; 2. Yes, at each scalar interval of the mapping.	1. Lognormal distribution type; 2. Cumulative distribution.
Additional distribution options	Volume normalisation: 1. Normalised to the original volume of non-porous particles; 2. Normalised with consideration of aggregate porosity.	Save the size distribution at regular time intervals: 1) Time, i = at regular intervals, e.g. "Time, 2", saves once every 2 sec. 2) Size, i = at regular intervals the average size of the aggregate as it evolves during the simulation, e.g. "Size, 10" saves once every 10 µm. 3) Size%, i = with regular percentage changes in the average size, e.g. "Size%, 20" saves once every 20%.

Table 7 continues. Description of the option windows of the display parameter field.

Parameter	Option box 1	Option box 2
Mean aggregate diameter	Display: 1. Yes, but on completion 2. Yes, and start the display.	Save the results of the previous run: 1. Of the last start-up; 2. The last two runs
Energy dissipation rate		
Shear rate		
Viscosity	Display: 1. Yes, but on completion 2. Yes, and start displaying	Save the results of the previous run: 1. The last start-up; 2. The last two starts
Porous aggregate volume frac.		
Mixing Index		
Flocculant degradation		
Pipe Reynolds' Number		
Mudline settling flux		
Check mass conservation		

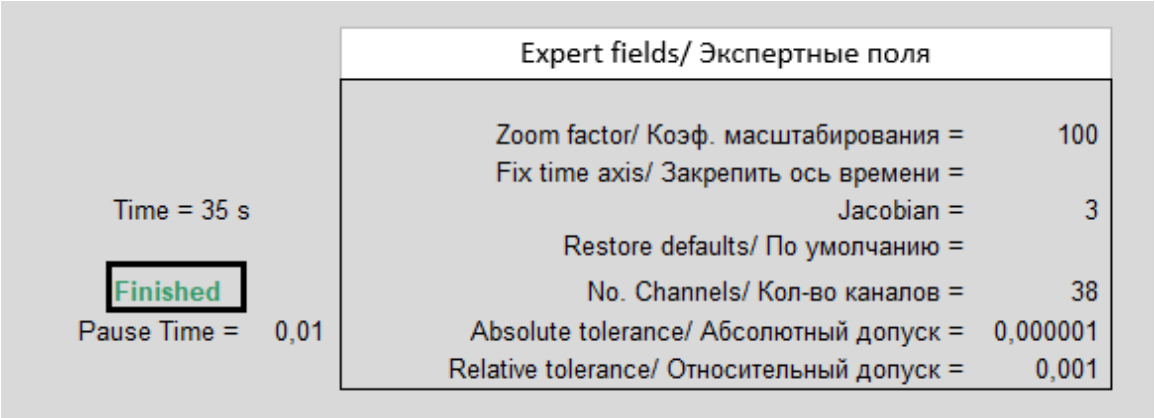

Figure 39. Expert field

The particle size distribution is plotted as cumulative distributions or "bell-shaped" distributions. In a bell-shaped distribution, the particle size is plotted on the x-axis and the number, mass fraction or percentage of particles in each size range is plotted on the y-axis.

This graph is actually a bar graph (vertical bar chart). However, a point is usually placed in the centre of each size channel and the points are combined to produce a smooth bell-shaped distribution. This type of graph makes it easier to see the shape of the particle distribution, the proportion of fines, etc.

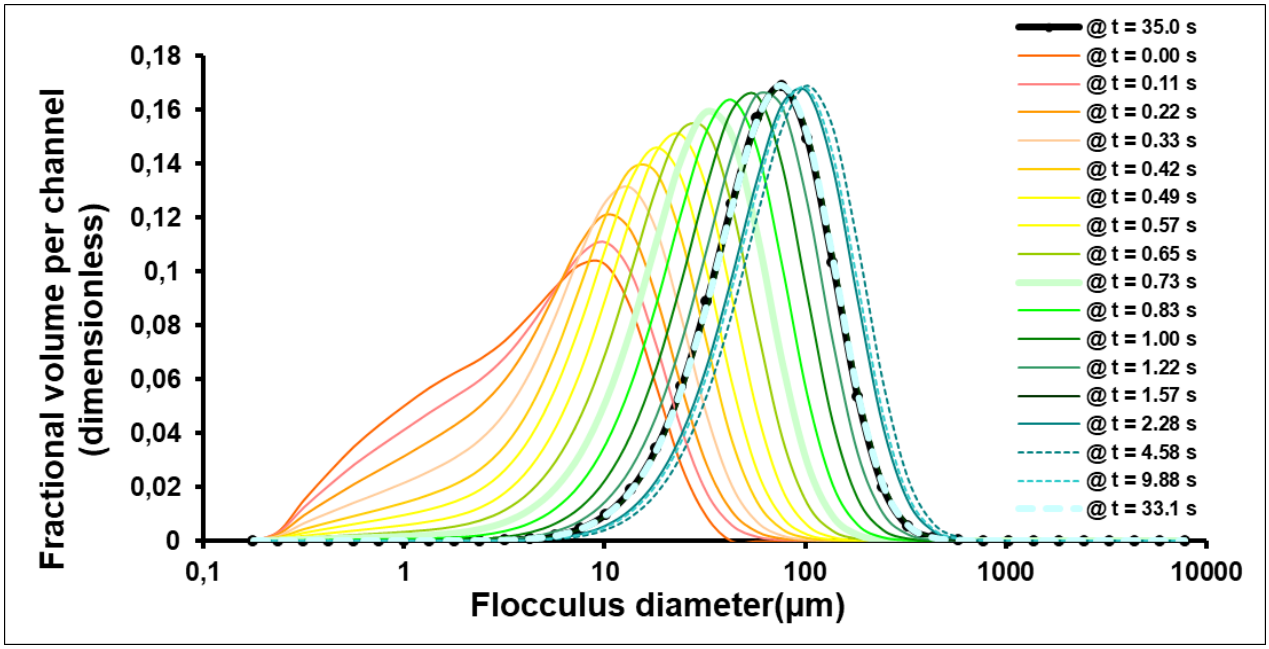

Figure 40. Aggregate/flocculus diameter distribution

In the flocculation diameter distribution graph, it can be seen that the volume fraction of medium-sized particles has decreased, but the volume fraction of larger particles has increased. The reason why the distribution becomes narrower comparatively is that the flocculation process tends to bring the aggregates to an overall stable size. Smaller aggregates aggregate into larger aggregates, while larger aggregates are less stable and more likely to be broken up.

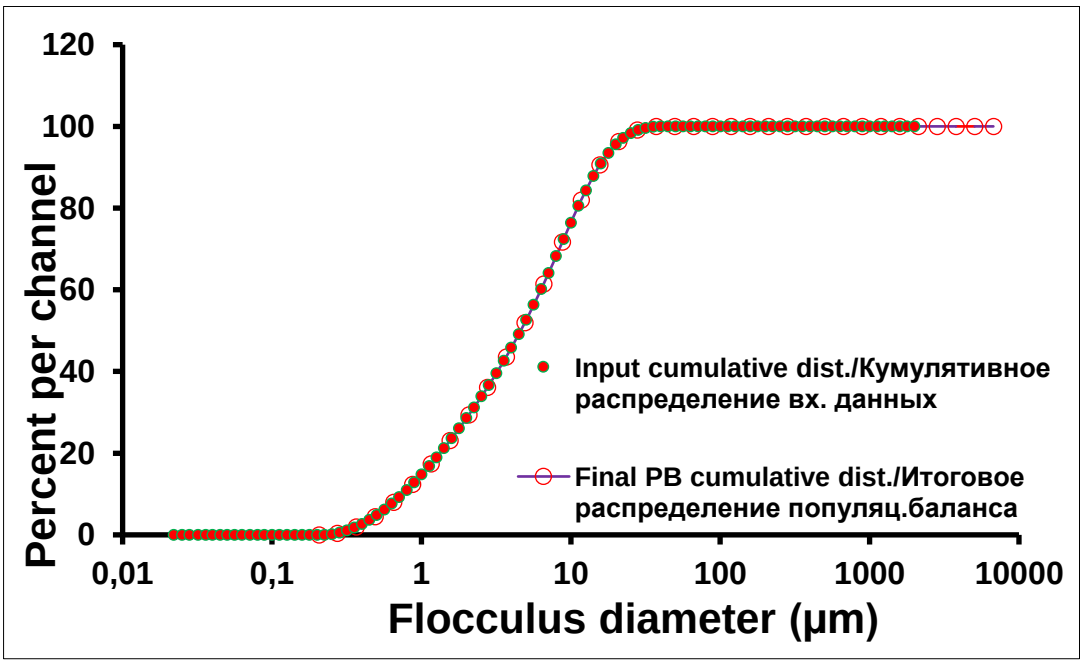

Figure 41. Generated cumulative particle distribution

The cumulative distribution, on the other hand, is plotted as a pass percentage as a function of particle size; this uses the top size of each size channel rather than the centre size.

For example, in sieve sorting, the cumulative distribution is easily obtained by working up the sieve sizes, plotting the cumulative mass as a function of the sieve mesh size. Converting the cumulative distribution into a bell-shaped distribution requires interpolation between the sieve sizes to obtain the average particle size caught between each pair of sieves.

Particle size distributions are usually highly skewed, with a long tail stretching towards larger sizes to the right. Therefore they are usually plotted with a logarithmic x-axis and size ranges whose width gradually increases according to the numerical progression. This makes the distribution more symmetrical, and often the particle size distributions are described by a lognormal distribution. In addition, the size distribution can be plotted with the number of particles or even the surface area on the y-axis, but it is more usual to plot the percentage by mass in each size range. This takes into account the fact that only a few large particles may contain most of the sample mass. To generate very large aggregates it is possible to increase the number of channels and thus constrain the distribution. This adjustment will make the model run slower, so only 38 channels are used by default.

4.1 Conclusion

During the fourth chapter of the master's work, the software code for monitoring the particle size distribution of the focussed slurry was developed and an interface was used to easily correct the calculations and visualize the results.

`Cumulative particle size distribution and aggregate diameter distribution plots were obtained. The particle size distribution was plotted as a "bell-shaped" distribution, where the particle size (diameter) is plotted on the x-axis and the percentage content on the y-axis, which demonstrates the correct description of the flocculation model and application of the population balance model.

5. ECONOMIC PART

On the basis of the analysis of the existing conditions at the plant to identify problems and subsequent patent search to find solutions the following problems and methods of their solution have been identified.

Thus, in relation to the investigated unit it was noted insufficient effective control of the object, which led to the emergence of emergency situation during which there was an overflow of solid fraction in the thickener. The thickener must be stopped and cleaned if this situation occurs. The whole process of restoring the thickener to a usable state takes on average two days. There is no exact data on the frequency of emergencies, but it should be noted that these shutdowns are not scheduled and cannot be accounted for in the plant schedule. It is then assumed that a downtime of two days occurs once every 4 months.

The proposed solution to incorporate the monitoring system alorithm into the existing system involves modifying the control loop in operation and adding a large number of parameters that will be displayed on the SCADA system and allow the operator to have a clear view of the state of the unit at any time, which, in turn, will help to eliminate emergency situations caused by ineffective control, in other words to eliminate downtime of the unit.

A positive economic effect is the elimination of downtime, by increasing the capacity compared to the current capacity. However, it is worth noting that there are other positive effects of this solution: more efficient flocculant aid consumption and reduced filter load. However, these effects cannot be accounted for by the available data, so they are not included in the following calculation.

The first thing to do is to estimate the purchase costs of the necessary equipment. For example, the approximate cost of instrumentation and controller modules is shown in the table below.

Table 8. Equipment costs required

Automation system element		Qty	Cost (RUB)
Analogue input module	SM331 (6ES7 331-7NF10-0AB0)	2	189868,68
Analog output module	SM332 (6ES7 332-5HF00-0AB0)	1	103010,04
Digital input module	SM-321 (6ES7 321-1BL00-0AA0)	1	40874
Digital output module	SM-322 (6ES7 322-1BL00-0AA0)	1	56595
Temperature sensor	ДТС015М -50М.0,5.120.И	1	3 174
Coriolis flowmeter	F025S 113C0AMEZAZZ	1	109500

Table 9 continues. Equipment costs required

Automation system element		Qty	Cost (RUB)
Electromagnetic flowmeter	ПРОФИ – 122ММО	2	90000
Current sensor	T201	2	9220
Weight sensor	JUMO 404387/0-491-405515-20-601-06	1	10000
Density sensor	FMG60 - A2A1A2G2A1A	1	10950
Bed level sensor	FineTek EGX10000A1AIA501MAS300A0AB00050-5500	1	20000
Turbidity sensor	Seli STS 03	1	191167,5
Total			**834359,22**

The next step is to calculate the economic effect of eliminating one emergency situation.

Thus, knowing the nominal value of feed flow Q_{feed}=365 m3/h and flow rate of thickened product Qout=95 m3/h it is possible to calculate the flow rate of liquid phase discharge, in other words, aluminate solution, which will then turn into finished product - alumina. To go to the mass flow rate the following information will also be required:

F_{ifeed} - 0.0175 vol - solid content of the feed slurry

Fi_{out} 0.06 fractions - solids content of thickened product

q_s - 3200 kg/m3 solid phase density

q_l - 1240 kg/m3 liquid phase density

qs_{ol} - 1420 kg/m3 density of clarified solution

Then, the mass flow rate of the feed and the mass flow rate of the thickened product are equal:

$$G_{feed} = Fifeed \cdot q_{тв} \cdot Q_{feed} + (1 - Fifeed) \cdot q_{ж} \cdot Q_{feed} \quad (17)$$

$$G_{out} = Fiout \cdot q_{тв} \cdot Q_{out} + (1 - Fiout) \cdot q_{ж} \cdot Q_{out} \quad (18)$$

G_{feed} = 465441,43 kg/h

G_{out}=128972 kg/h

Knowing the mass flow rates of all other material flows, the mass flow rate of the thickener discharge can be calculated.

$$G_{cl} = G_{feed} - G_{out} \quad (19)$$

$$G_{cl} = 336469 \text{ kg/h}$$

Then, the mass flow rate of the liquid per day will be 8075266.32 kg/day. However, this is not yet the finished product, but the mass of the aluminate solution. In order to find the mass of the finished product, the regulatory value of aluminium concentration in the aluminate solution C_{Al}=145.15 g/l or 145150 g/m3 is used.

To calculate the alumina capacity, the volume occupied by the daily weight of aluminate produced by the thickener must be calculated.

$$Q\_cl = G\_cl/q\_l \quad (20)$$

$$Q_{cl} = 5686{,}81 \text{ m}^3\text{/day}$$

The daily output of the thickener can now be calculated in terms of finished product.

$$Q_{cl} \cdot C_{Al}/1000000 \quad (21)$$

$$Gfp = 825.4 \text{ t/day}$$

The last step to estimate the economic effect is to convert the mass of finished products into a monetary equivalent. For this purpose, we used data from the annual report of RUSAL on the amount of products produced by the Ural aluminium plant for 2020.

And also information from the article "Calculation of the expected economic efficiency of aluminium production by increasing the use of domestically produced alumina" by A.V. Alexandrov and N.V. Nemchinova, which indicates the approximate cost per tonne of alumina in production at RUSAL's domestic facilities for 2020. Thus, the total cost per tonne of alumina would be $248.26.

The cost of sales per tonne of alumina for 2020 can also be obtained from the annual report of RUSAL, it is equal to 278 dollars.

Since, in the future, this value will often be used immediately to calculate the net profit from the sale of one tonne of alumina. Then, profit before tax will be $29.74, and net profit 23.792 dollars, or at the current rate of 73.48 rubles will amount to 1,748 rubles.

With all this data, you can proceed to the calculation of payback proposed in this work.

The costs to be spent are the sum of the purchase of equipment and downtime unit due to start-up of the new system. Let's assume that it takes five full days to install the equipment and start up the unit. Then, the total cost of the proposed solution will be:

834359,22 rub +(825,4 t/d · 5 d·1749 rub)= 8052832,675 rub

Thus, net cash flows are presented in Table 2.

Table 10 . Net cash flows

Year	0	1	2
FCF	-8052833	+8662168	+8662168

Then, the net present value will be

$$NPV = \sum \frac{FCF}{(1+k)^i} - I_0 \quad (22)$$

$$NPV = \frac{8662168}{1{,}13} + \frac{8662168}{1{,}13^2} - 8052832{,}675 = 6396551 \text{rub, NPV>0}$$

Internal rate of return:

$$-I_0 + \sum \frac{FCF}{(1+IRR)^i} = 0 \quad (23)$$

IRR=0,71

Profitability index:

$$PI = 1 + \frac{NPV}{I_0} \quad (24)$$

$$PI = 1 + \frac{6396551}{8052833} = 1{,}79\text{, PI>1}$$

Discounted payback period:

Table 11. DPBP calculation

DFCF	-8052833	+7665635	+6783748
Balance	8052833	387197	0
Year	0	1	2

5.1 Conclusion

In the course of work on the economical chapter of the master's work, the annual report of UAZ RUSAL OJSC was studied. An analysis was made of the existing factors that could be improved by introducing a virtual flocculated slurry monitoring system device into the ACS.

The proposed solution will fully pay for itself in the first month of the second year, which is a good payback period for an investment project in the metal industry.

Based on the calculated figures, it can be said that the implementation of the proposed solution is cost-effective and economically efficient

6. CONCLUSION

To conclude, the main objectives of the work have been achieved. In the course of the study and in particular in the conduct of the experiment, difficulties were encountered due to limited laboratory conditions. In the future, it is planned to repeat the experiment in order to obtain clear images of the red slurry slurry to create synthetic data in Blender software. The synthetic data will then be used as the basis for machine learning of the particle size distribution monitoring system.

The developed software part of the flocculation population balance model will be duplicated in python programming language, to obtain adequate thickener model in ANSYS, in which the first stage of thickening process - pulp flocculation - will be considered, as all patented models assume that solid fraction is not taken out from above and model considers thickener in free and constrained settling zones.

7. SUMMARY

The introduction of digital systems in metallurgical production facilities is among the most advanced research activities. It is not possible to solve the problem of particle sizing without direct interference in the technological process without the use of a virtual instrument.

In the course of the master's work, a literature review and analysis of existing research on the topic was carried out to confirm the relevance of the master's work. In particular, the following aspects of special and practical parts were touched upon: study of technological process of red mud thickening, study of process and kinetics of flocculation, application of population balance. A laboratory study of flocculation of red mud slurry was carried out on a sample obtained from UAZ RUSAL's production in 2020. The practical part concludes with the implementation of the software code of the monitoring system and its visual component.

The economic part considers the feasibility of implementing the monitoring system at UAZ RUSAL JSC.

REFERENCES

1. Dr. Alan Rawle. "Basic principles of particle size analysis", [Web site]. [Accessed 10 March 2021]. Available at: https://pel.spb.ru/.

2. JSC «SCMA». “Facility for Continuous Automatic Measurement of Particle Sizes in a Slurry Flow "PIK-074P"(U)”, [Web site]. [Accessed 10 March 2021]. Available at: https://scma.com.ua/.

3. Buriko, A.V. 2017. Digital Evolution, or Why Rusal Is Going Digital. Digital Production, No. 2, P. 18-23. [Accessed 10 March 2021].

4. Trifonova. P 2019, "TMK will create its own digital twin", Vedomosti, 19.06.2019, [Online], [Accessed 10 March 2021], Available at: https://www.vedomosti.ru/.

5. Bazhin, V.Y. Digital automated complexes in electrometallurgy of aluminum: textbook. Polytech-Press Publisher, 2021. [Accessed 10 March 2021].

6. Skorin I., Kozlov V.E., Stadnik V.V. 2003. Virtual Instruments of Measurements, [Accessed 10 March 2021].

7. Venkataramana Runkana, P. 2006. A Population Balance Model for Flocculation of Colloidal Suspensions Incorporating the Influence of Surface Forces. / Venkataramana Runkanaa, P. Somasundarana, P.C. Kapurb // Chemical Engineering Science 61 (2006) 182 – 191. [Accessed 16 March 2021].

8. Heath, Alex R. Combined population balance and CFD modeling of particle aggregation by polymeric flocculant / Alex R. Heath, Peter T.L. Koh, A.J. Parker // Cooperative Research Centre for Hydrometallurgy (CSIRO Mine-als) . – Clayton South, Victoria, Australia. – Third International Conference on CFD in the Minerals and Process Industries CSIRO. – Australia. – 2003. – 6 p. [Accessed 16 March 2021].

9. Golberg, G.Y., 2019. Development of the theory of formation and destruction of flocculation structures in the processes of separation of suspensions of fine coal enrichment products, Ph. D., IPCON RAS, Moscow. [Accessed 16 March 2021].

10. Dueñas Díez, M., 2004. Population balance modeling and passivity-based control of particulate processes, applied to the Silgrain process., PhD., Telemark University College Faculty of Technology Porsgrunn, Norway. [Web source]. – Available at: https://core.ac.uk/download/pdf/52104063.pdf. [Accessed 23 March 2021].

11. Naumchik A.N., Dubovikov O.A.,1987. "Production of alumina from low-quality raw materials: a training manual": L., ed. LGI, 1987, 99 p. [Accessed 23 March 2021].
12. Fedorova E. R., 2017. Distribution of feed flow between parallel thickeners in controlling the technological limit of thickening and washing of red mud of alumina production, Ph.D., St. Petersburg Mining University, St. Petersburg. [Accessed 23 March 2021].
13. Nopens, I, 2002. Modelling the activated sludge flocculation process combining laser light diffraction particle sizing and population balance modelling (PBM). / I. Nopens, C.A. Biggs, B. De Clercq, R. Govoreanu, B.-M. Wilén, P. Lant and P.A. Vanrolleghem // Water Science and Technology. – 2002. – V. 45, № 6. – P. 41-49 [Accessed 16 March 2021].
14. Glover, S. M., 2001, Polymer Molecular Weight and Mixing Effects on Floc Compressibility and Filterability / S.M. Glover, Y.D. Yan, G.J. Jameson and S. Biggs // 6th World Congress of Chemical Engineering. Melbourne. – 2001. [Accessed 16 March 2021].
15. Li Feng., 2017. Fabricating an anionic polyacrylamide (APAM) with an anionic block structure for high turbidity water separation and purification/ Li Feng, Huaili Zheng, Baoyu Gao, Shixin Zhang, Chuanliang Zhao, Yuhao Zhou, Bincheng Xu // Royal Society Chemistry Advances. – 2017, № 7. – P. 28918-28930. [Accessed 16 March 2021].
16. Jiangya Ma., 2017, Flocculation properties and kinetic investigation of polyacrylamide with different cationic monomer content for high turbid water purification/ Jiangya Ma, Kun Fua, Xue Fua, Qingqing Guanc, Lei Dinga, Jun Shia, Guocheng Zhud, Xinxi Zhanga, Shihua Zhanga, Liyan Jia // Separation and Purification Technology. – 2017, № 182. – P. 134-143. [Accessed 16 March 2021].
17. Biggs, S. 1998, The Fractal Analysis of Aggregates Formed via a Bridging Flocculation Mechanism/ Simon Biggs, Michael Habgood, Graeme J. Jameson and Yao-de Yan // Proceedings of the 26th Australian Chemical Engineering Conference (Chemeca 98), Port Douglas, Australia. – 1998. [Accessed 16 March 2021].
18. Spicer P.T., 1997, Shear-Induced Aggregation-Fragmentation: Mixing and Aggregate Morphology Effects: PhD Thesis / P.T. Spicer. – Cincinnati: University of Cincinnati, 1997. – 283 P. [Accessed 16 March 2021].
19. Walaszek, W., 2006, Porosity and interior structure analysis of pellet-flocs/ W. Walaszek, P. Ay // Colloids and surfaces A: Physicochemical and Engineering Aspects. – 2006. – V. 280, №№ 1-3. – P. 155-162. [Accessed 16 March 2021].

20. Ahrens, R., 2020, Efficient numerical treatment of aggregation integrals in multivariate population balance equations: PhD Thesis. Technischen Universität Hamburg – 2020. [Web source]. – Available at: https://tore.tuhh.de/handle/11420/6907. [Accessed 16 March 2021].
21. Barthelmes, G., Pratsinis S.E, Buggisch, H., 2003, Particle size distributions and viscosity of suspensions undergoing shear-induced coagulation and fragmentation. Chemical Engineering Science. – 2003; 58(13):2893-902. [Accessed 12 March 2021].
22. RUSAL URAL Financial Results Report, 2020. [Accessed 24 March 2021].
23. CSIRO. P266F 1-D Sedimentation Model Manual. – 2008.

LIST OF GRAPHIC MATERIAL

LIST OF TABULAR MATERIAL